Assessment of the floor response spectra due to pounding between adjacent structures during earthquakes: an alternative approach to study local amplifications

B. Bodnar, T. Heitz, J. Clément, B. Richard

▶ **To cite this version:**

B. Bodnar, T. Heitz, J. Clément, B. Richard. Assessment of the floor response spectra due to pounding between adjacent structures during earthquakes: an alternative approach to study local amplifications. Engineering Structures, 2022, 255, pp.113922. 10.1016/j.engstruct.2022.113922 . hal-03727499

HAL Id: hal-03727499
https://cnam.hal.science/hal-03727499

Submitted on 26 Aug 2022

HAL is a multi-disciplinary open access archive for the deposit and dissemination of scientific research documents, whether they are published or not. The documents may come from teaching and research institutions in France or abroad, or from public or private research centers.

L'archive ouverte pluridisciplinaire **HAL**, est destinée au dépôt et à la diffusion de documents scientifiques de niveau recherche, publiés ou non, émanant des établissements d'enseignement et de recherche français ou étrangers, des laboratoires publics ou privés.

Distributed under a Creative Commons Attribution - NonCommercial - NoDerivatives 4.0 International License

Assessment of the floor response spectra due to pounding between adjacent structures during earthquakes: an alternative approach to study local amplifications

B. Bodnar [a], T. Heitz [b], J. Clément [b], B. Richard [b,1]

[a] *LMSSC, CNAM, 292 rue Saint-Martin, 75003 Paris, France*

[b] *IRSN, 31 avenue du Général Leclerc, F-92260 Fontenay-aux-Roses, France*

Abstract

The capability of safety structures, systems and devices to withstand dynamic loadings (earthquakes, impacts, pounding, falling of heavy objects, etc.) is part of the design basis of nuclear power plants or facilities. In order to ensure their correct design, it is necessary to assess, beforehand, the admissible load. However, the validity of the Response Spectrum Analysis (RSA) largely used in the community can be legitimately questioned since it does not account for local high dynamic phenomena and is strongly dependent on the choice of parameters to get a satisfactory assessment of the calculation results.

In this paper, the reliability of the RSA to design devices in case of pounding loading is studied. An alternative approach to describe pounding between two adjacent structures during earthquakes is proposed, in order to assess the floor response spectra (FRS) with a reasonable computation time. The loading demand is then computed at the bottom of a device located at floor level, from a step-by-step calculation and by performing a RSA. The reliability of the RSA is assessed by comparison of these results.

To perform calculations, the impact forces are firstly assessed using linear beam models with the same modal characteristics as the ones of the building under study. Then, the pounding loading is applied to a three-dimensional mesh of the first structure made from shell and beam finite elements. The results highlight the propagation of shock waves and underline local amplifications of the FRS at the edges of the floors. The loading demand given by the RSA shows that the error related to the step-by-step calculation decreases when pounding is considered. It turns out that the impact loading leads to higher horizontal displacements and reduces rotations at floor level. Its amplitude increases when the damping of the structure is low, especially in the high frequency range. With an error of less than 10%, the RSA method may be regarded as acceptable in case of pounding between adjacent multi-storey buildings.

Keywords: civil engineering, earthquake engineering, numerical simulations, pounding between structures, floor response spectra, response spectrum analysis

[1] Corresponding author. (Benjamin Richard – benjamin.richard@irsn.fr).

1. Introduction

For nuclear power plants or facilities, the seismic responses of structures, systems and devices to the postulated design earthquakes are predicted by a detailed dynamic analysis or by equivalent testing procedures. The integrity of the safety-related devices of nuclear power plants must be assured in the event that earthquakes occur at nuclear plant sites. Further to the Fukushima accident, the robustness of the seismic design in the event of an earthquake significantly greater than the safe shut-down earthquake was re-examined. In particular, pounding between two adjacent structures is part of this technical reassessment. The periodic upward re-assessment of the seismic risk that may also be considered by local authorities (*e.g.* in the French territories) increases the amplitude of the response spectra used to design civil engineering structures [1]. As a result, according to current standards, the gap between two adjacent buildings may not be sufficient anymore to prevent them from pounding. These re-assessments drive operators to investigate on new analysis methods in order to evaluate safety margins.

In order to study earthquake induced pounding between two adjacent structures, it is necessary to look at impact modelling methods. Their development started with O'Hara (1959) who was the first to study the response spectra associated with impact loadings ([2] & [3]). Later, Kelly *et al.* (1979) developed various analytical models to assess the response of structures under impulse loadings [4]. Anagnostopoulos (1988) modelled the impact between two buildings under earthquake by using a penalty method [5]. Then, he proposed a model in which the energy dissipation due to impact was equated to an equivalent viscous damping [6]. Papadrakakis (1991) developed in parallel a numerical method based on the introduction of Lagrange multipliers to the dynamic equation [7], while Muthukumar (2006) used a Hertz contact model [8]. The work of Acary put forward the linear complementarity problem method (LCP), consisting in solving the dynamic balance equations in terms of velocities by modelling each impact as a jump in terms of quantity of motion ([9] & [10]). More recently, Crozet *et al.* (2019) compared the results given by a model based on the work of Anagnostopoulos with the results given by an experimental campaign carried out at the CEA (French Alternative and Atomic Energies Commission) [11]. The influence of the gap between both buildings on the floor response spectra (FRS) in pseudo-acceleration was investigated [12]. Finally, Langlade (2019) compared penalty method with the LCP method, including the influence of the input parameters. In particular, he showed that the linear complementarity approach converges with larger time steps than the penalty method [13].

Because impact modelling considerably increases computation times, its application to high-dimensional models involving a high number of degrees of freedom (DOF) remains a challenging task. Langlade (2019) and Crozet *et al.* (2018) chose to describe the structures using simplified beam models ([13] & [12]). However, this method, simple to implement, does not allow observing the propagation of shock waves at floor level nor modelling complex impact areas. Other researchers used frame models made of beam and surface elements, such as Jameel *et al.* (2012) [14], Mahmoud *et al.* (2013) [15], Yang *et al.* (2019) [16] and Zhang *et al.* (2019) [17]. These approaches, much more accurate, require modelling entirely both pounding structures, which drastically increases the number of DOFs and the computation time. Lastly, Mazza et al. (2020) investigated on magnetic damped links to

reduce pounding in base-isolated buildings by means of simplified modelling strategies avoiding unwanted computational coasts [18]. To do so, a four-storey RC building with an elevator shaft damped by elastomeric bearings was modelled [19]. Torsional effects induced by an asymmetric position of the elevator shaft were investigated.

In order to assess the effect of pounding due to earthquakes at a floor level on which a device may be located, the so-called "transferred spectrum method" is conventionally used. It consists in computing the dynamic response at the floor levels, by means of a simplified linear beam model of the building. The response obtained is then used (in the same way as in earthquake engineering) to determine, by a post-processing technique, the FRS at the floor of interest, making possible the assessment of the pseudo-acceleration experienced by the device to be studied. The loading demand is then computed by applying the Response Spectrum Analysis (RSA) method. In this case, the floor response is assumed to be spatially uniform.

The main advantage of this method is its ease of implementation (compared to detailed 3D finite element analyses). However, its ability to account for dynamic loading that are faster than earthquakes (collisions, impacts) is still an open question for several reasons. Firstly, the construction of a spectrum is only applicable, in theory, when the acceleration is homogeneously distributed over the entire structure. This assumption is reasonable, for example, when a building is subjected to a seismic loading, but needs to be checked in case of impact loadings, which generate shock waves that propagate through the floors. Secondly, the resulting FRS are characterized by very high peak floor accelerations (PFA). However, these very high pseudo-accelerations are associated with small displacements (below one millimeter). In practice, some anchors could not meet such a displacement. The applicability of design methods employing FRS (such as RSA) can thus be legitimately questioned with respect to the loading demand computed from the results of step-by-step detailed 3D finite element analyses.

In this paper, an alternative approach to assess pounding between two adjacent structures is proposed. The flowchart of the proposed approach is depicted in Figure 4 (see Section 3.2). To illustrate the method, the pounding between two multi-storey buildings representative of typical nuclear power plant (NPP) facilities is assessed. A realistic scenario is considered, to make feasible the assessment (*via* a simple case study) of the proposed alternative method allowing for the identification of the FRS on a 3D structure.

Firstly, the virtual case study is presented. Secondly, the simplified beam models (SBM) and the method used to model pounding are detailed. In the third part, the resulting impact forces are applied to the 3D mesh of the first building, allowing for the assessment and the analysis of the local displacement and pseudo-acceleration FRS. Finally, the reliability of the RSA method classically used to design the devices and their anchors is assessed. To do so, a device is added to the 3D mesh.

2. Presentation of the case study

Both buildings are 30.93 m high, from the foundations to the upper part of the acroterion. They are made of 8 levels (including 1 foundation level, 1 basement and 6 storeys). Their foundations are rectangular in shape and each occupies a 46.20 × 15.60 m²

area. The study focuses on the 8th storey, where impacts are more likely to occur. The mass centre of this floor is located at a height of 30.30 m from the foundations.

Walls are between 60 cm and 100 cm thick, and storey are between 3.20 m and 4.50 m high (except for the basement which is only 2.32 m high - *cf.* Figure 1 (b)). Slabs are 30 cm thick and each one is supported, in the transversal direction, by 7 rows of beams whose cross-section is 75 × 85 cm² and, in the longitudinal direction, by beams whose cross-section is 20 × 28 cm². Loads are transmitted to the foundations at mid-width thanks to 7 columns whose cross-section is 80 × 120 cm². Most bays are included to the sidewalls, as shown in Figure 1 (a). The area of each one of them is given in Table 1 (according to the indices defined in Figure 1 (b)).

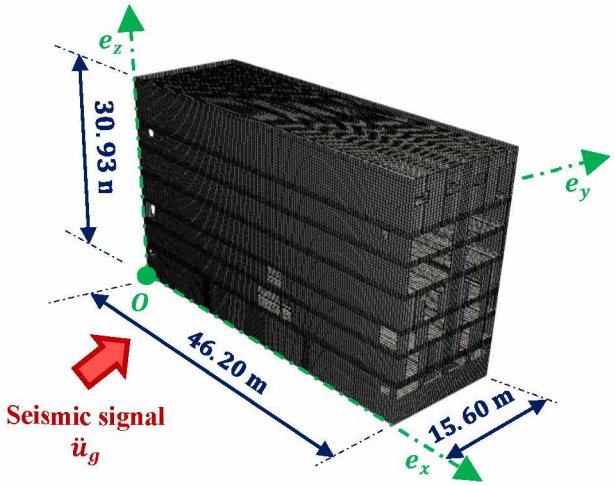

(a)

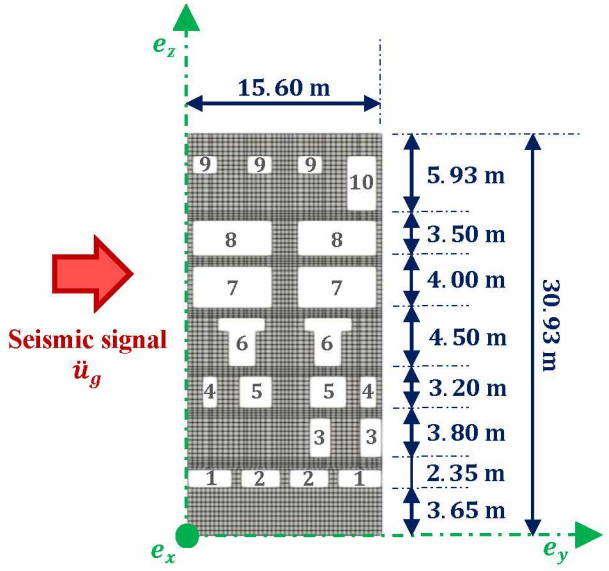

(b)

Figure 1 : 3D mesh of the first building (a) and sidewall (b).

The building is made of reinforced concrete. A Young modulus of 33 GPa, a Poisson ratio of 0.18 and a density of 2400 kg/m^3 are considered. Here, no live load is applied to the floors, so only the dead loads (*i.e.* related to the weight of the structure) are taken into account to perform seismic analyses. Total masses of floors are given in Appendix A and used to define the SBMs. An accurate mesh of the first structure made of 113051 shell and beam elements is shown in Figure 1.

Table 1: Areas of bays in each sidewall.

Index of the bay	Location(s)	Area
1	Basement	330 × 57 cm^2
2	Basement	300 × 57 cm^2
3	1st storey	120 × 300 cm^2
4	2nd storey	90 × 210 cm^2
5	2nd storey	240 × 210 cm^2
6	3rd storey	330 × 90 cm^2 (upper part) 200 × 270 cm^2 (lower part)
7	4th storey	580 × 320 cm^2
8	5th storey	580 × 270 cm^2
9	6th storey	160 × 120 cm^2
10	6th storey	160 × 395 cm^2

The first building is stiffer than the second one, while the masses applied to the floors are the same on both. To model earthquake induced pounding, a gap of 1 cm between the two buildings is considered (*cf.* Figure 2 (a)). Note that this value belongs to the same order of magnitude that cases tested by Crozet *et al.*, with a gap worth between 0 and 5 cm [11]. This simplistic case study (parallelepiped buildings subjected to a symmetrical loading) is used to assess the validity of the method allowing for the identification of the local FRS due to pounding.

The seismic signal is drawn in Figure 2 (b) and applied in the transverse direction. Its PGA is 2.32 m/s^2 and is reached at time 3.16 s. It is an artificial signal typical of a French average (close to strong) seismic hazard area, with a PGA between 1.6 m/s^2 and 3.0 m/s^2 (according to [20]). Its strong phase lasts 3 s, from time 2 s to time 5 s. The pseudo-acceleration FRS is plotted in Figure 2 (c) at ground level with a damping ratio equal to 5 % and compared to the elastic design spectrum (computed for a distant earthquake of type 1 with a magnitude more than 5.5 impacting high importance buildings on a stiff soil with a low energy dissipation). Its maximum value is reached at 5.12 Hz and is 7.17 m/s^2.

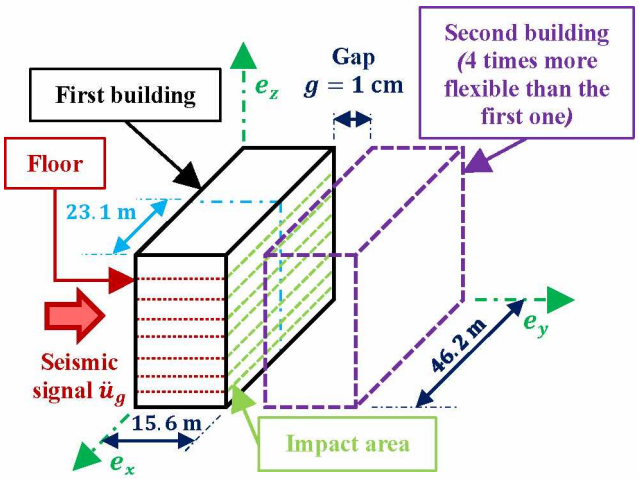

(a)

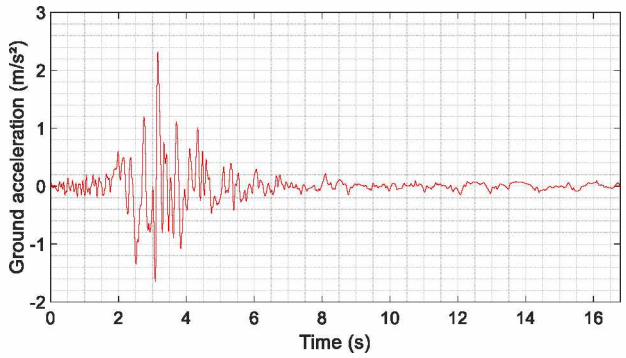

(b)

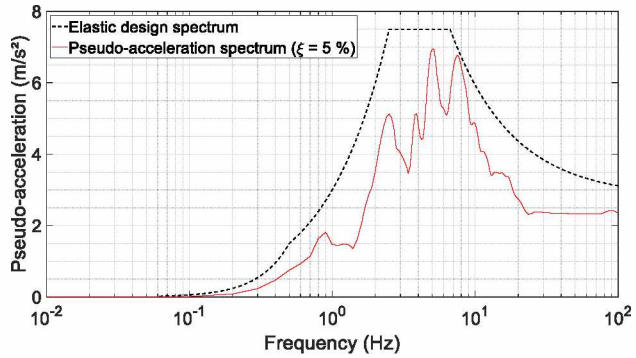

(c)

Figure 2 : Configuration of the case study (a), ground acceleration (b) and response spectrum of ground-motion with a 5 % damping ratio (c).

Building modelling is firstly made with simplified beam models (SBMs) made of Timoshenko beam elements in order to assess the impact forces applied to the 3D mesh. The first SBM has the same modal characteristics as the ones of the 3D mesh, whereas the second moments of area of the second SBM are arbitrarily four times lower. The modal properties of the SBMs, the penalty method used to model impacts, and the response of the simplified beam models are detailed in the following section.

3. Simplified models used to compute impact loadings due to earthquake induced pounding

3.1 Geometry and modal characteristics of the SBMs

The geometrical and mechanical properties of the SBMs (shown in Figure 3 (b) for the first structure) depend on the masses of the floors as well as the modal characteristics of the buildings. The floors being significantly stiffer than walls and columns, they are set as rigid structural components, the first three eigenmodes being mainly due to wall bending (as pictured in Figure 3 (a), showing the first bending mode shape of the 3D model). Consequently, the eigenfrequencies of the SBMs do not depend on the stiffness of the floors.

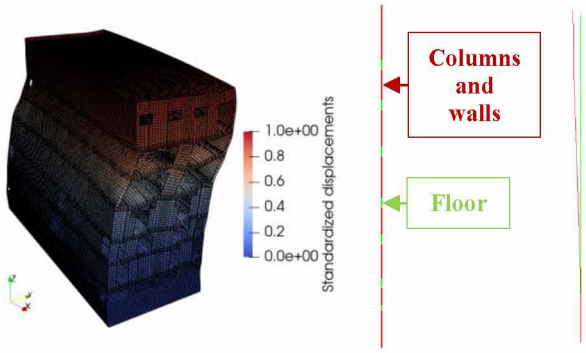

(a) (b) (c)

Figure 3 : First bending mode shape of the 3D model - f = 1.80 Hz (a), SBM (b) and first bending mode shape of the SBM - f = 1.75 Hz (c).

The effects of shear on displacements are taken into account using Timoshenko beam elements. Each floor is modelled by three nodes, connected by two rigid beam elements, respectively located at:

- the lower edge of cross beams;
- the mass centre of each floor;
- the upper edge of cross beams.

On the first building, the second moments of area of the storeys are set to guarantee that the first three bending modes in the direction of the earthquake (*i.e.* rotation about $\boldsymbol{e}_x$ as shown in Figure 3 (c)) are close to the ones of the 3D mesh (*cf.* Figure 3 (a)). Indeed, both models must have the same masses and similar modal characteristics in order to compute representative impact forces. The first three eigenfrequencies of both models are compared in Table 2, whereas the effective modal masses are given in Table 3. The mechanical properties of floors and storeys (masses, stiffnesses, …) are summarized in Appendix A.

Table 2: Eigenfrequencies of the first building related to the first three eigenmodes of bending about $\boldsymbol{e}_x$.

Eigenmodes	3D mesh (Hz)	SBM (Hz)	Relative difference (%)
1	1.80	1.75	2.8
2	5.80	5.19	10.5
3	9.53	9.57	0.4

Table 3: Effective modal masses of the first building related to the first three eigenmodes of bending about $\boldsymbol{e}_x$.

Eigenmodes	3D mesh (t)	SBM (t)	Relative difference (%)
1	10,463	10,100	3.5
2	2,144	2,293	6.9
3	459	349	24.0

The second building is only modelled by a SBM, the local amplifications of the FRS at floor level being only studied on the first building. The second SBM is almost identical to the first one (the storeys have the same height and the floors carry the same masses), except that the second moments of area of the storeys are four times lower. The first three eigenfrequencies and effective modal masses of the second SBM are summarized in Table 4.

Table 4: Eigenfrequencies and effective modal masses of the second SBM (first three eigenmodes of bending about $\boldsymbol{e}_x$).

Eigenmodes	Eigenfrequency (Hz)	Effective modal mass (t)
1	1.29	9,165
2	4.44	3,098
3	9.64	451

Table 2 shows that the relative error between the eigenfrequencies of both models does not exceed 11 %. In addition, the relative error between the effective modal masses does not exceed 7 % for the two first eigenmodes and 24 % for the third one. The sum of the modal masses of the first three eigenmodes of bending is 13,066 t for the 3D mesh and 12,742 t for the SBM (in both cases, more than 81 % of the mass above ground level is carried by these eigenmodes). The error between both models being only 324 t (*i.e.* 2.5 % by comparison with the 3D mesh, see Table 3), the SBMs are thus suitable to assess impact forces, provided that floor

deformations and energy dissipation at impacts (due to the damping ratio applied to the floors) are taken into account. To do so, the penalty method is used, as described in the following.

3.2 Definition of impacts according to the penalty method

3.2.1 Principle and description of the penalty method

Impacts have been studied by several authors over the last decades. Among them, Anagnostopoulos (1988) [5] and Crozet *et al.* (2018) [12] modelled impacts between two SBMs by connecting adjacent floors with Kelvin-Voigt chains. The impacts are thus taken into account by using the penalty method, *via* a nonlinear elastic stiffness (*i.e.* defined by a zero value in tension and a high value in compression). The energy dissipation due to impacts is approximated by means of a viscous damping ratio. The use of a penalty stiffness reduces the dependency of impact forces on the time step in the high frequency range. Impact forces and acceleration peaks are thus continuous and finite (contrary to the LCP method [9]), making it possible to apply the impact forces to the 3D meshes as external loads. Moreover, even if the amplitude of the impact forces is highly dependent on the modelling parameters (penalty stiffness, time-step…), the viscous damping ratio is set so that the jump in quantity of motion before and after each impact remains proportional to the energy restitution ratio ε [6] (modelling the loss of kinetic energy). The response given by both penalty and LCP method is thus almost identical, provided that the penalty stiffness is high enough, as the number of calculation times during impacts [13].

As a result, because it allows to compute continuous impact forces, a classical penalty method is chosen to model impacts on the SBMs. Its application to pounding problems is detailed in this section, while the procedure used to assess and apply impact forces to the 3D meshes (which is one of the original contributions of this paper) is summarized in the flowchart in Figure 4. Note that this method was developed in order to study the pounding between two buildings with floors located at the same height. Otherwise, it is necessary to add intermediate nodes so that each level faces an adjacent node.

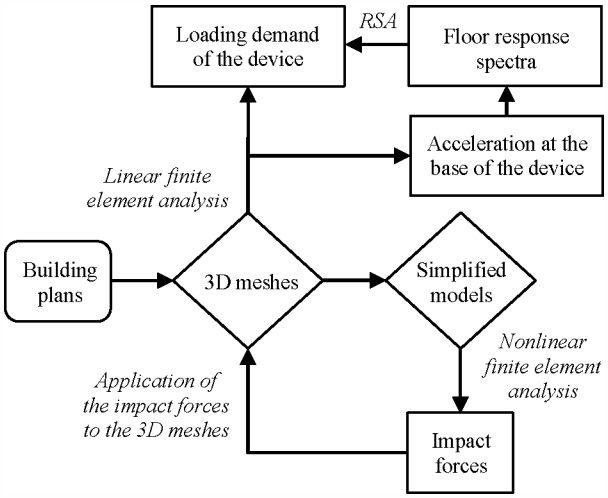

Figure 4 : Alternative approach used to assess the forces applied to a device in a structure subjected to earthquake induced pounding.

The penalty method consists in introducing (when an impact occurs) a vector of impact forces whose components depend on an infinite elastic stiffness (compared to the one of the structures) to the equilibrium equation (1).

$$\boldsymbol{M}\cdot\ddot{\boldsymbol{u}}+\boldsymbol{C}\cdot\dot{\boldsymbol{u}}+\boldsymbol{K}\cdot\boldsymbol{u}=\boldsymbol{f}^{ext}+\boldsymbol{f}^{c} \qquad (1)$$

where $\boldsymbol{M}$ is the mass matrix, $\boldsymbol{C}$ the viscous damping matrix, $\boldsymbol{K}$ the elastic stiffness matrix, $\boldsymbol{f}^{ext}$ and $\boldsymbol{f}^{c}$ the vectors of external and impact forces, and $\ddot{\boldsymbol{u}}$, $\dot{\boldsymbol{u}}$ and $\boldsymbol{u}$ the acceleration, velocity, and displacement vectors.

By considering that pounding occurs between two SBMs made from N_b adjacent floors spaced from each other by a gap g (*cf.* Figure 5), the global system has $N = 2 \times N_b$ nodes. The components of $\boldsymbol{f}_{i+1}^{c}$ in the direction of $\boldsymbol{e}_y$ (noted f_y^c) are thus defined according to (2).

$$\begin{cases} \left(f_{y,i+1}^{c}\right)_k = K_{Ceq}\cdot\left(\Delta u_{y,i}\right)_k + C_{Ceq,k}\cdot\left(\Delta\dot{u}_{y,i}\right)_k \\ \left(f_{y,i+1}^{c}\right)_{k+\frac{N}{2}} = -K_{Ceq}\cdot\left(\Delta u_{y,i}\right)_k - C_{Ceq,k}\cdot\left(\Delta\dot{u}_{y,i}\right)_k \end{cases} \quad \text{if } \left(\Delta u_{y,i}\right)_k < 0 \qquad (2)$$

$$\begin{cases} \left(f_{y,i+1}^{c}\right)_k = 0 \\ \left(f_{y,i+1}^{c}\right)_{k+N/2} = 0 \end{cases} \quad \text{if } \left(\Delta u_{y,i}\right)_k \geq 0$$

where K_{Ceq} (in N/m) and $C_{Ceq,k}$ (in kg/s) are the elastic stiffness and the viscous damping coefficient taken into account to model impacts [6], $(\Delta u_{y,i})_k = (u_{y,i})_{k+N/2} - (u_{y,i})_k + e$ the length of interpenetration depending on the gap g between both buildings, and $(\Delta \dot{u}_{y,i})_k = (\dot{u}_{y,i})_{k+N/2} - (\dot{u}_{y,i})_k$ the relative velocity between adjacent floors in the direction of $\boldsymbol{e}_y$ (*cf.* Figure 5).

Note that index i represents the computation time, k the floor and N the total number of nodes. Displacements indexed k and $k + N/2$ are thus linked *via* face-to-face nodes belonging to different oscillators.

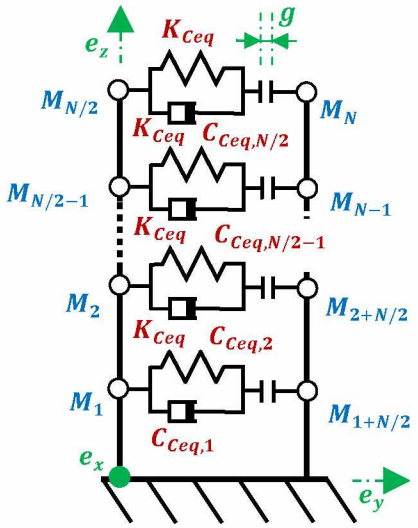

Figure 5 : Modelling of impacts between two SBMs.

The viscous damping coefficient of each floor is defined such that $C_{C,k} = 2 \cdot \xi_c \cdot \sqrt{K_{Ceq} \cdot M_k}$ (with ξ_c the viscous damping ratio at impact). According to [6], the viscous damping coefficient $C_{Ceq,k}$ to consider between two adjacent floors of masses M_k and $M_{k+N/2}$ is thus defined by (3).

$$C_{Ceq,k} = 2 \cdot \xi_c \cdot \sqrt{K_{Ceq} \cdot \frac{M_k \cdot M_{k+N/2}}{M_k + M_{k+N/2}}} \qquad (3)$$

Note that the value of ξ_c (without unit) is computed in order to guarantee a jump in velocity (before and after each impact) such that $\dot{u}^+ = -\varepsilon \cdot \dot{u}^-$, with ε the energy restitution ratio (without unit), worth between 0 (soft impact) and 1 (hard impact). As a result, it comes:

$$\xi_c = \frac{-\ln(\varepsilon)}{\sqrt{\pi^2 + \ln^2(\varepsilon)}} \qquad (4)$$

When impacts are taken into account, irregularities and discontinuities appear during dynamic finite element analyses. In order to achieve viable results, relevant parameters need to be used. However, ε and K_{Ceq} depends on many factors, such as the materials, the shape of the impact area and the relative velocity of floors [21]. Without experimental studies, it is impossible to accurately assess these coefficients: they are thus defined as calibration parameters based on the properties of the 3D mesh. A method allowing for their assessment is described in the following section.

3.2.2 Choice of the calculation parameters

In order to guarantee that both the 3D mesh and the SBM have a similar behaviour, the penalty parameters ε and K_{Ceq} have to be in accordance with the mechanical and geometrical properties of the RC floors. Knowing that the masses of the floors are extremely large (over 1500 tons), it is expected to have significant deformations at the vicinity of impacts, leading to a dissipation of energy when the floors are damaging. Therefore, ε cannot be taken as one to model actual structures with the SBMs. Calculations being performed by assuming a linear elastic behaviour for both buildings, all the dissipations are here modelled by using a Rayleigh viscous damping ratio applied to the entire 3D mesh. When impacts occur on the 3D mesh, a part of the energy is thus lost due to the Rayleigh damping at floor level. In addition, the penalty stiffness K_{Ceq} has to be set in order to correctly model floor deformations with the SBMs.

Note that pounding being rarely taken into account for industrial purpose, authors chose to not model damage and pounding at the same time, even if structural damage can be important in a comprehensive assessment of earthquake induced pounding (especially around impact areas where the penalty parameters depend on the damage of concrete). Interaction between pounding and damage could be investigated into a further study by using nonlinear beam elements with global damage laws ([22] & [23]) or multifibre beam elements with local damage laws [24]. However, the evolution of the restitution ratio according to the damage of the impact areas and the velocity is still an open question [25].

An accurate 3D mesh of the first building being available here, a method allowing for the assessment of ε and K_{Ceq} is proposed. To do so, the impact forces are computed under the assumption that pounding occurs between the 3D mesh of the first building and a rigid wall. An initial displacement equal to - 2 cm is applied to the 8th floor: the boundary condition is then released, allowing the structure to move freely until the gap of 1 cm between the impact areas and the rigid wall is reached. The floors being explicitly modelled, the linear complementarity method (LCP) is used instead of the penalty method to model impacts on the 3D mesh (the wall being rigid, no penalty stiffness nor restitution ratio needs to be added). Kinematic boundary conditions are applied to nodes located along the length and the height of the 6th, 7th, and 8th floors (where impacts are more likely to happen).

The Rayleigh viscous damping ratio (noted ξ) is set at 7.0 % at f_1 = 1 Hz and f_2 = 20 Hz. On the SBMs, the damping is applied to each storey in order to reach a low around the main eigenmodes (due to bending here), whereas only the terms related to the mass matrix are taken into account at floor level (β_R is thus equal to zero on the green elements in Figure 3 (b)). This conservative

value is in accordance with the French nuclear authority (ASN) if used to perform linear finite element analyses [26], as it is the usual engineering practice. The viscous damping matrix is thus defined such as $\boldsymbol{C} = \beta_R \cdot \boldsymbol{K} + \alpha_R \cdot \boldsymbol{M}$, so coefficients α_R and β_R are computed according to [27] as functions of f_1 and f_2, leading to $\alpha_R = 0.8378$ s^{-1} and $\beta_R = 0.0011$ s. The frequencies f_1 and f_2 are thus set in order to guarantee a reasonable damping ratio (between 4 % and 7 %) around the first bending modes, as it has been done to perform linear finite element analyses on the 2008 SMART benchmark [28]. It should be noted that it is also possible to use a Caughey damping ratio to decrease the damping in the high-frequency range [29].

To ensure the convergence of the results, an average acceleration Newmark-beta method (implicit and unconditionally stable) is used, *i.e.* $\beta = 1/4$ and $\gamma = 1/2$ (parameters of the Newmark-beta method). The finite element analysis is performed over the time interval [0 s, 1.3 s] using Cast3M® software. Here, a maximum value of 50,000 calculation time-steps has been chosen to assess impact forces on the SBMs according to the available computer processing unit (CPU). The duration of the seismic signal being 16.79 s, the resulting time step Δt is thus 0.34 ms. The same value is used to model impacts on the 3D mesh. The resultant of the impact forces applied to the 8th floor is thus computed over time and used as reference to find the best set of penalty parameters (*cf.* Figure 6 (a)).

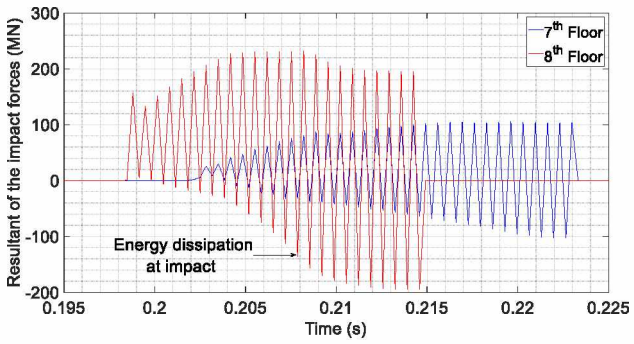

(a)

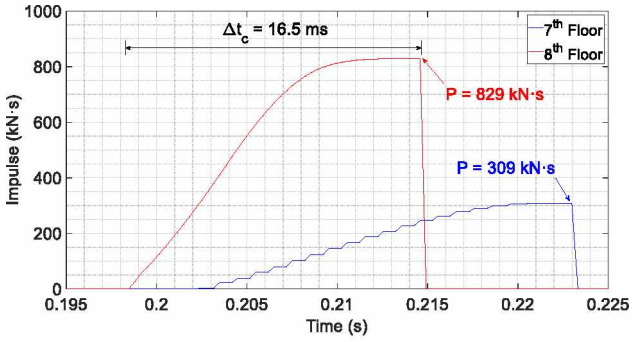

(b)

Figure 6 : Resultant of impact forces applied to the 8th floor (a) and resulting impulse (b) versus time.

Figure 6 (a) shows that one impact is applied to the 7th and 8th floor. It appears on floor at time 198 ms and lasts approximately 16.5 ms. Due to the Rayleigh viscous damping, the sign of the forces is reversed at the end of the impact, leading to an energy

dissipation. To find the best fitting penalty parameters at floor level, the resulting impulse (*i.e.* jump in terms of quantity of motion) is assessed by integrating over time the resultant of the impact forces (*cf.* Figure 6 (b)). Its maximum value P is equal to 829 kN·s, and can be expressed for a unilateral impact such as $P \approx M \cdot \dot{u}^- \cdot (1 + \varepsilon)$, where M is the mass applied to the floor, $\dot{u}^-$ the velocity of the mass centre before the impact, and ε the restitution ratio. So, it comes:

$$\varepsilon \approx \frac{P}{M \cdot \dot{u}^-} - 1 \tag{5}$$

The velocity $\dot{u}^-$ before the impact is 0.163 m/s (*cf.* Figure 7 (b)), while the total mass of the 8th floor is 3014 t. As a result, $\varepsilon \approx 0.687$. This value is in agreement with Crozet, who suggests that the energy restitution ratio ε between two reinforced concrete floors is worth between 0.67 and 0.84, depending on the pre-impact velocity [21]. This value is also close to the choice of Langlade (2021) [25], who used a restitution ratio equal to 0.6 based on a post-processing of the experimental results of Crozet (2019) [11].

A penalty stiffness about 1000 times greater than the one of the buildings is commonly used to model impacts [12]. However, since the simplified models have 6 DOFs per node, the evaluation of a representative stiffness remains difficult. But Anagnostopoulos (1988) showed that the duration of the unilateral impacts of a SDOF tends to $\Delta t_c = \pi/\Omega_D$ with $\Omega_D \approx \sqrt{K_{Ceq} \cdot (1 - \xi_c^2)/M}$ when $K/K_{Ceq} \to +\infty$ (with K the representative stiffness of the oscillator) [5]. Knowing the duration of the impact, it comes:

$$K_{Ceq} \approx \frac{M}{1 - \xi_c^2} \cdot \left(\frac{\pi}{\Delta t_c}\right)^2 \tag{6}$$

According to (4), ξ_c is approximately equal to 0.129. As a result, $K_{Ceq} \approx 1.1 \times 10^{11}$ N/m. The finite element analysis is thus performed on the SBMs by using $K_{Ceq} = 10^{11}$ N/m (order of magnitude of the penalty stiffness). All floors having the same stiffness and geometrical properties, the same set of penalty parameters is used on each storey.

Note that the time step Δt has a great influence on the numerical results. To be able to correctly assess the impact forces, it is necessary to ensure a sufficient number of calculation times per impact. Knowing that at least 8 points are necessary to correctly describe the period of an oscillatory phenomenon, it can be reasonably considered that guaranteeing at least 16 computation times per impact make it possible to achieve a satisfactory convergence of the result. By considering that $\Delta t \leq \pi/(16 \cdot \Omega_D)$, it comes:

$$\Delta t \leq \frac{\pi}{16 \cdot \sqrt{1 - \xi_c^2}} \cdot \sqrt{\frac{M}{K_{C_{eq}}}} \tag{7}$$

Knowing that the lightest floor weighs 1574 t, $\Delta t \leq 0.79$ ms. This condition is largely complied with $\Delta t = 0.34$ ms, which guarantees a minimum of 36 calculation times per impact (with $\Delta t_c \geq 12.5$ ms $\ll 16.79$ s). The calculation parameters used to perform finite element analyses on the SBMs are summarized in Table 5.

Table 5 : Summary of the calculation parameters.

E (GPa)	ν (-)	ε (-)	ξ_c (-)	K_{Ceq} (N/m)	e (cm)	Δt (ms)
33	0.2	0.69	0.12	10^{11}	1.0	0.34

The reliability of the penalty method applied to the SBMs is assessed by comparison with the previous results (*i.e.* LCP method applied to the 3D mesh). To do so, displacement, velocity, and impulse are computed in the direction of $\boldsymbol{e}_y$ at the mass centre of the 8th floor. Figure 7 (a) shows that the first impact appears almost at the same time on both models (with a delay of 11.1 ms with the SBM). As expected, its impulse and duration remain almost the same (*cf.* Figure 7 (c)), showing that the method used to assess the penalty parameters is suitable. According to Figure 7 (a) and Figure 7 (b), the SBM matches with the 3D mesh in terms of displacement and velocity, even if the displacement peaks are slightly overestimated on the SBM: as a result, a second impact appears at time 0.737 s. However, the second impulse (equal to 37 kN·s) being 21 times lower than the first one, it does not significantly affect the response of the building. This shows that the SBMs can be used with the penalty parameters summarized in Table 5 to correctly assess the impact forces applied to the 3D mesh. The application of this method to earthquake induced pounding is detailed in Section 3.3.

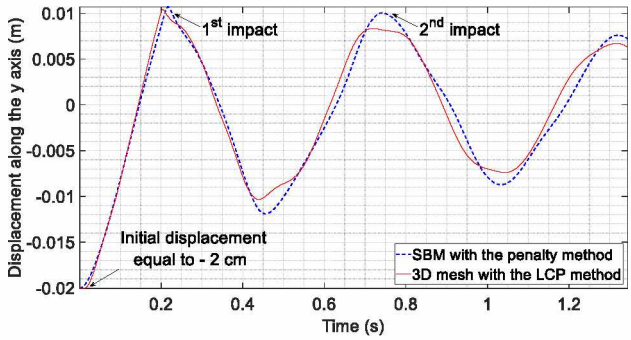

(a)

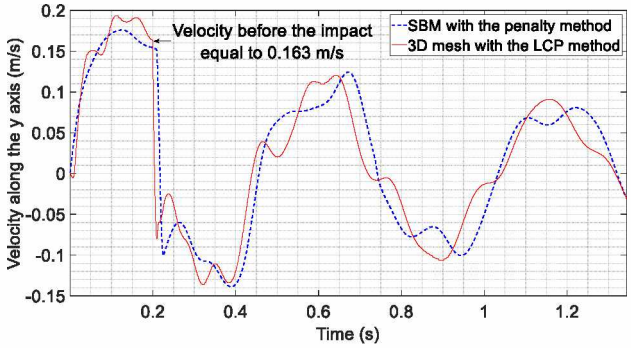

(b)

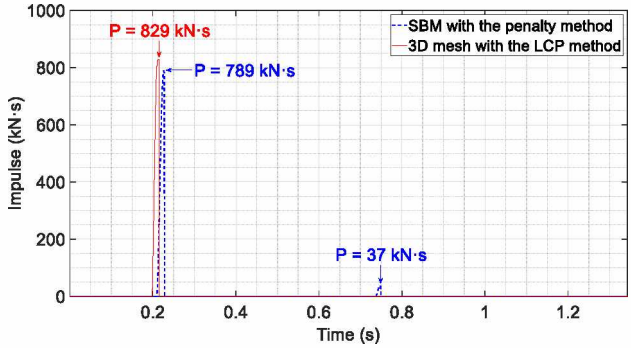

(c)

Figure 7 : Displacement (a), velocity (b), and impulse (c) responses in the direction of $\boldsymbol{e}_y$ at the centre of mass of the 8th floor versus time.

3.3 Modelling of earthquake induced pounding between the SBMs

In this section, the earthquake induced pounding between both buildings is modelled on Cast3M® software by using the SBMs with the penalty method. The displacement, velocity, acceleration and gap in the direction of $\boldsymbol{e}_y$ are plotted versus time at the mass centre of the top floors in Figure 8, while the impact forces are shown in Figure 9.

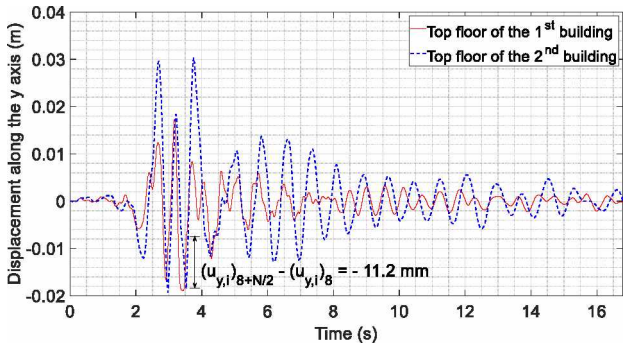

(a)

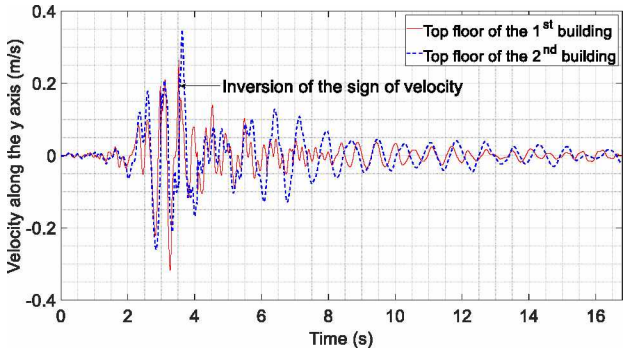

(b)

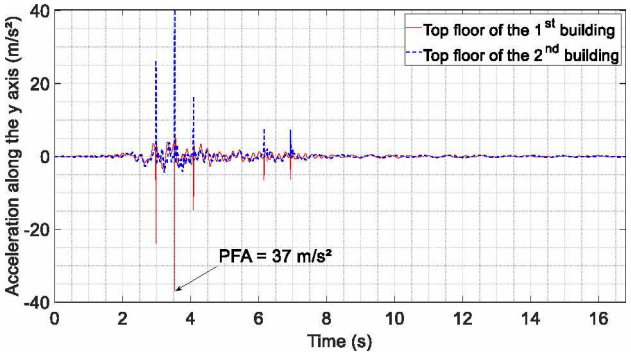

(c)

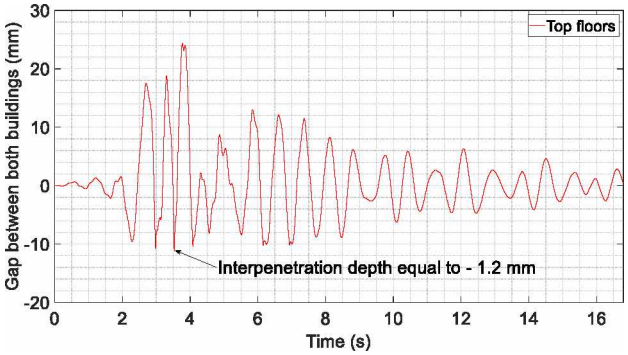

(d)

Figure 8 : Displacement (a), velocity (b), and acceleration (c) responses in the direction of $\boldsymbol{e}_y$ at the top floors (indexed k = 8) and gap between both buildings (d) versus time.

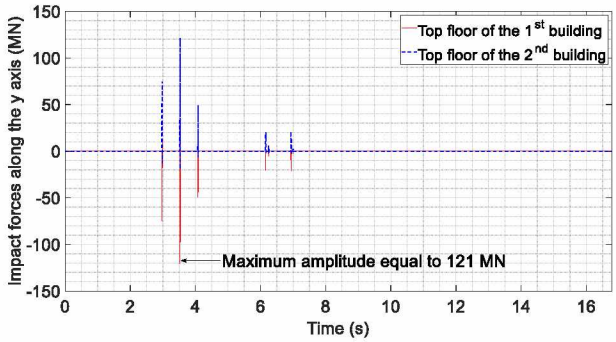

(a)

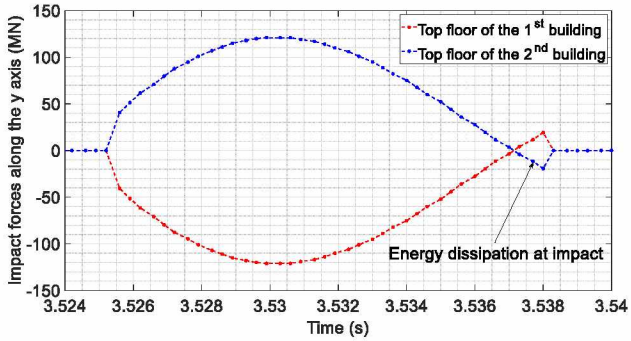

(b)

Figure 9 : Impact force applied to the top floors (a) and main impact force (b) versus time.

Figure 8 (d) shows that the interpenetration depth between both top floors $(\Delta u_{y,i})_{k=8} = (u_{y,i})_{8+N/2} - (u_{y,i})_8 + e \leq 0$ reaches - 1.2 mm at time 3.532 s (with $k = 8$ the index related to the top floors, see Section 3.2.1). As shown in Figure 8 (a), this value remains weak compared to the maximum amplitude of the displacements (around 2 cm for the first building and 3 cm for the second one). Moreover, Figure 8 (c) highlights that each impact generates an acceleration peak whose duration remains negligible in comparison with the duration of the seismic signal (lasting 16.79 s). These acceleration peaks (reaching 37 m/s² at time 3.532 s) have a large amplitude, each impact bringing a considerable amount of energy and leading almost instantaneously to reverse the velocity of the floors (*cf.* Figure 8 (b)).

In addition, according to Figure 9 (a), the impact force reaches 121 MN at time 3.532 s (maximum value). By looking at this peak, Figure 9 (b) shows that the penalty method makes it possible to compute continuous loading with impact forces distributed over several computation times and not depending on the time step. This avoids numerical instabilities and allows the temporal interpolation of the loading applied to the 3D mesh. Note that the sign of the force changes at the end of the impact, leading to an energy dissipation. This phenomenon only appears when ε is less than 1 (so ξ_c has a non-zero value). With 38 calculation times during the main impact (lasting 13.1 ms and occurring at time 3.532 s), the time step Δt is small enough to accurately assess the amplitude of impact forces in case of earthquake induced pounding.

The construction of the FRS is carried out at each floor by considering a 5 % damping ratio at the anchors of the device (*cf.* Figure 10). The calculations were performed between 0 Hz and 500 Hz by applying the Nigam and Jennings method (1968), which

consists in analytically computing the response of the device assuming that the acceleration evolves linearly between each time step [30]. Figure 10 shows that the impacts (occurring at the 7th and 8th floors) increase the pseudo-acceleration in the high frequency range (*i.e.* $f \geq 30$ Hz). However, it stabilizes at the PFA of the floor response when $f \to +\infty$. Impacts generating quasi-instantaneous impulse loads, the FRS at the 7th and 8th floors reach high values in the high-frequency range (with 63.8 m/s² at 72 Hz at the 8th floor). Note that the FRS computed from the 1st to the 6th floor (where there is no impact) are similar to classical FRS assessed without pounding (*i.e.* with a lower amplitude in the high frequency range).

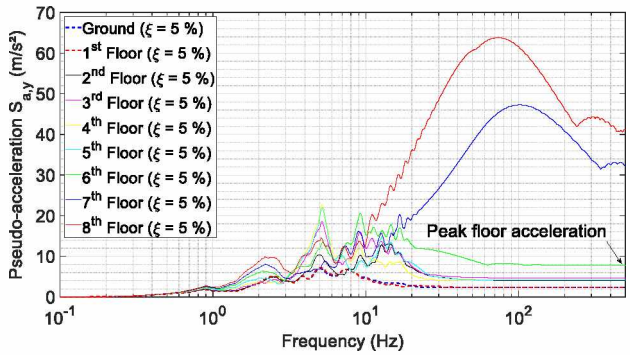

Figure 10 : FRS in pseudo-acceleration in the direction of $\boldsymbol{e}_y$ (penalty method with $K_{Ceq} = 10^{11}$ N/m and $\xi_c = 0.12$).

4. Application of the impact forces to the 3D mesh

4.1 Modelling assumptions

In order to identify the local amplifications of the FRS at floor level, the impact forces given by the SBMs (*cf.* Figure 11) are now applied to the 3D mesh of the first building (*cf.* Figure 1 (a)) using Cast3M® finite element software. In order to validate the results given by the simulation carried out on the 3D mesh, the response of the mass centre of the 8th floor is computed and compared to the results of the finite element analysis performed on the SBMs. The local FRS are then assessed at the 8th floor (according to the distance to the impact area), but also along the height of the building (at impact areas). To explain why local amplifications appears on the FRS, a study based on the transfer functions and the power spectral densities (PSD) of the impact forces is proposed.

The 3D mesh is made from 113251 shell and beam elements. The new finite element analysis is performed on 10,001 calculation times over the time interval [0 s, 10 s], so the response is sampled at 1000 Hz (*i.e.* $\Delta t = 1.00$ ms). The impacts are modelled as external loads distributed linearly along the impacting edge of floors, so impact detection is not performed on the 3D mesh. A larger time step can thus be used, decreasing CPU time.

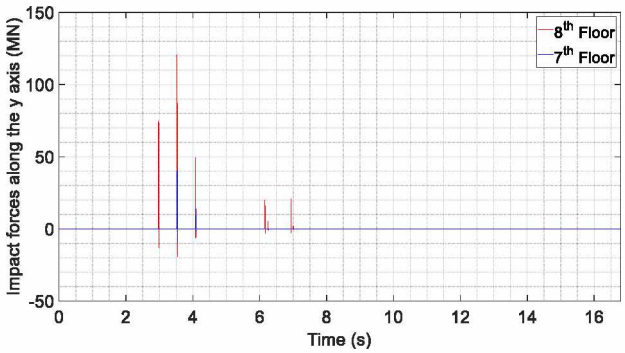

Figure 11 : Impact forces applied to the 3D mesh versus time.

The effects of torsion on impact forces are neglected here, even if the building is not fully symmetrical. Indeed, in case of earthquake, some torsional vibrations could appear. So, the impacts between two floors are not expected to be central and impact forces should not be uniformly distributed. The accuracy of the proposed method is thus highly affected from such torsional effects, which depend on the irregularities of the buildings.

However, firstly assessing the impact forces using SBMs before applying them on the 3D mesh allows to highly decreases the number of DOFs since only one building is modelled. The time-step can also be higher because impact detection is not necessary when impact forces are known, saving CPU time (the time step being 3 times larger here). Calculation times lasting usually less than 12 hours in design office, the method proposed in this paper could thus be used by engineers to design devices with a reasonable computational cost.

4.2 Response at the mass centre of the 8th floor

The response of the 3D mesh is computed in the direction of $\boldsymbol{e}_y$ by post-processing. Displacement and acceleration of the mass centre of the 8th floor are plotted versus time in Figure 12 while the pseudo-acceleration FRS is shown in Figure 13. The consistency of these results is assessed by comparison with the response of the SBM. Here, the acceleration peaks due to the impacts appear clearly (*cf.* Figure 12 (b)), and both models have the same behaviour in the high-frequency range (*cf.* Figure 13), even if the pseudo-acceleration is slightly higher on the 3D mesh (with a maximum value reaching 68.1 m/s² at 91 Hz).

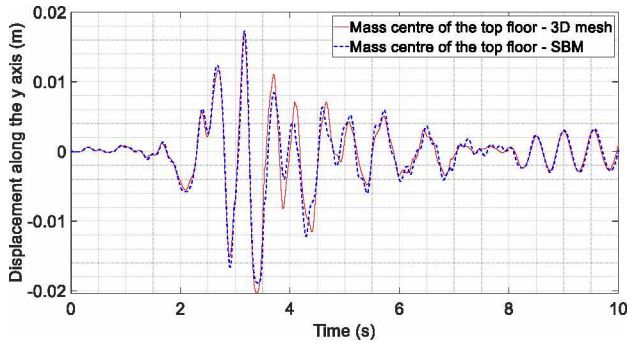

(a)

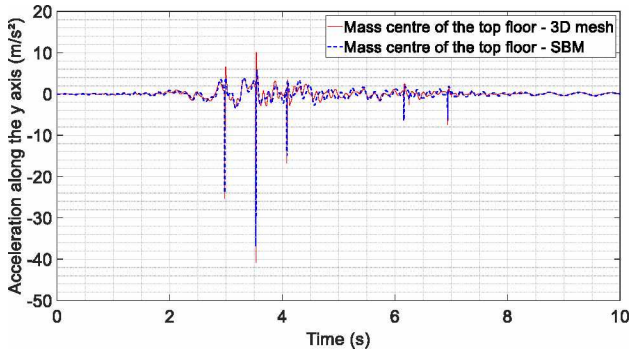

(b)

Figure 12 : Displacement (a) and acceleration (b) in the direction of $\boldsymbol{e}_y$ at the mass of the 8th floor versus time.

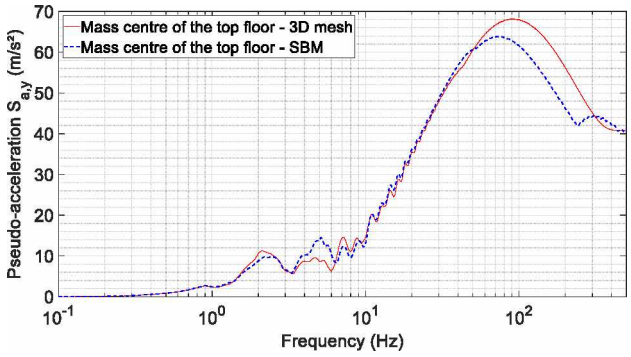

Figure 13 : Pseudo-acceleration FRS computed in the direction of $\boldsymbol{e}_y$ at the mass centre of the 8th floor.

4.3 Evaluation of FRS

4.3.1 Influence of the distance to the impact area

Impacts due to pounding generate a non-uniform acceleration field. This leads to the propagation of shock waves, making difficult to assess locally the behaviour of the device. In order to study the influence of the distance d between the device and the impacts area, the pseudo-acceleration FRS are computed:

- at each floor level. In this case, the studied points are located on the straight line oriented in the direction of the $\boldsymbol{e}_z$ axis and crossing the point of coordinates (23.1 m, 15.6 m, 0.0 m) (*i.e.* middle of the façade adjacent to the 2nd building);
- at the 8th floor. The studied points are thus located on the straight line oriented in the direction of the $\boldsymbol{e}_y$ axis and crossing the point of coordinates (23.1 m, 15.6 m, 30.3 m).

All these points are shown in Figure 14. The influence of the horizontal distance from the impact area as well as the influence of the height of the floor (to which the device is anchored) are studied in this section.

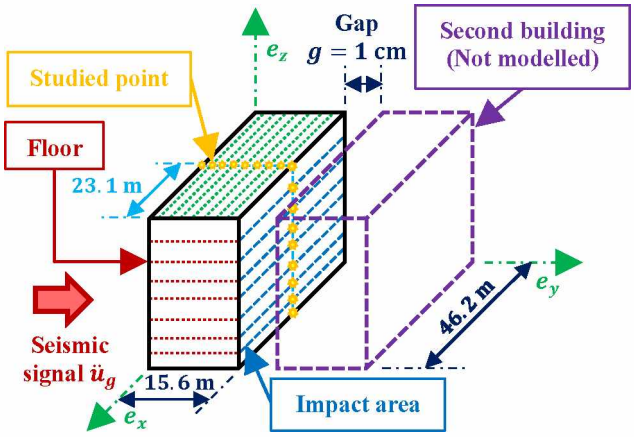

Figure 14 : Location of the points where the local FRS are assessed.

The FRS assessed at the 8th floor are given in Figure 15. This chart shows that the amplitude of the response depends on the position as the eigenfrequency of the device. When the eigenfrequency is less than 75 Hz, the floor response is maximum far from the impact areas. On the other hand, the pseudo-acceleration close to the impact areas is maximum around 85 Hz. Finally, when the eigenfrequency tends to the infinity (*i.e.* $f \to +\infty$), the highest PFAs are located at the edges of the 8th floor. At these locations, the FRS exceed 110 m/s². These high values are due to the propagation of transversal shock waves along the floor, leading to local increases in stress and acceleration when reflections happen. In order to understand why the pseudo-acceleration is more important at these locations, it is first necessary to look at the temporal floor response during the main impact (*cf.* Figure 16).

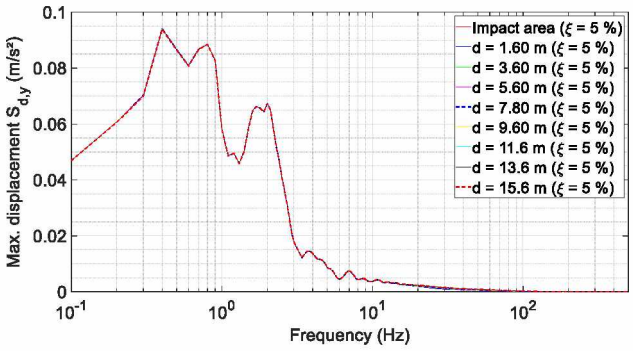

(a)

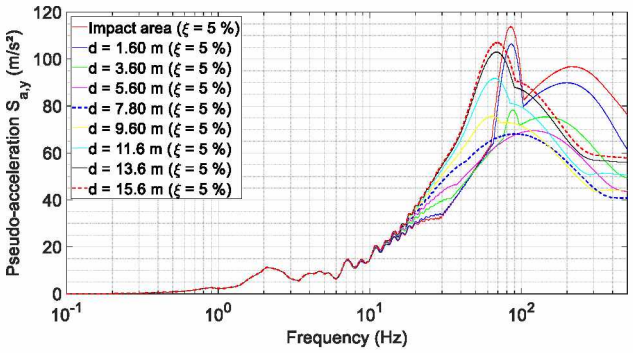

(b)

Figure 15 : FRS computed in the direction of $\boldsymbol{e}_y$ at the 8th floor: displacement (a) and pseudo-acceleration (b).

Figure 16 (b) shows that the main impact generates shock waves that travel to the opposite edge of the floor. When an edge is reached by a wave, all the energy is reflected, generating a local increase in stress and acceleration. Knowing that the velocity c_T of the shock waves is defined in (8), it comes c_T = 2345 m/s² (according to the data summarized in Table 5).

$$c_T = \sqrt{\frac{E}{2 \cdot \rho \cdot (1 + \nu)}} \qquad (8)$$

The building being 15.6 m large, each wave crosses the floor in T = 6.7 ms. So, two reflections happen while an impact of duration Δt_c = 13.1 ms occurs.

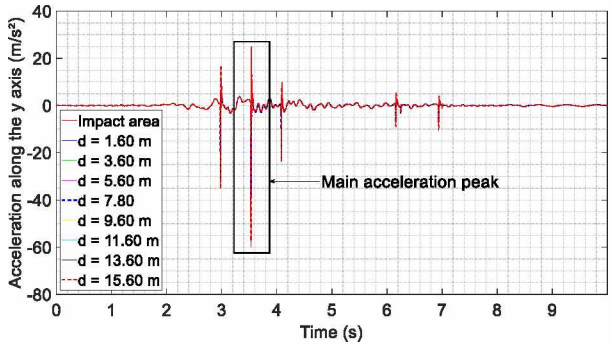

(a)

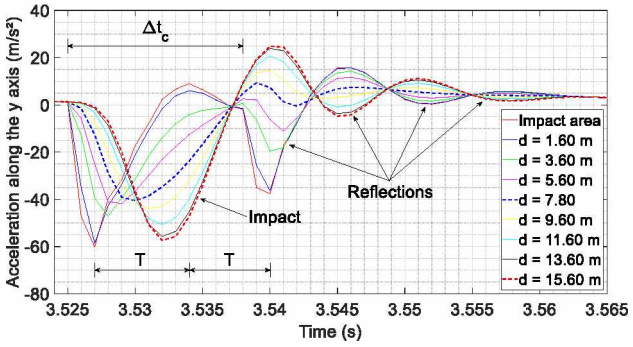

(b)

Figure 16 : Acceleration in the direction of $\boldsymbol{e}_y$ at the 8th floor versus time (a) and focus on the main acceleration peak (b).

The propagation of the transversal shock waves is described in Figure 17, showing the horizontal acceleration $\ddot{u}_y$ of each node belonging to the 8th floor. Figure 17 (d) shows the evolution of $\ddot{u}_y$ along the straight line oriented in the direction of $\boldsymbol{e}_y$ and crossing the point of coordinates (23.1 m, 15.6 m, 30.3 m). Note that floor deformations are amplified by a factor 2,000.

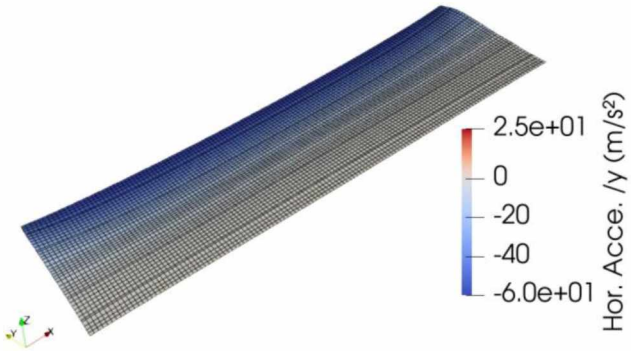

(a)

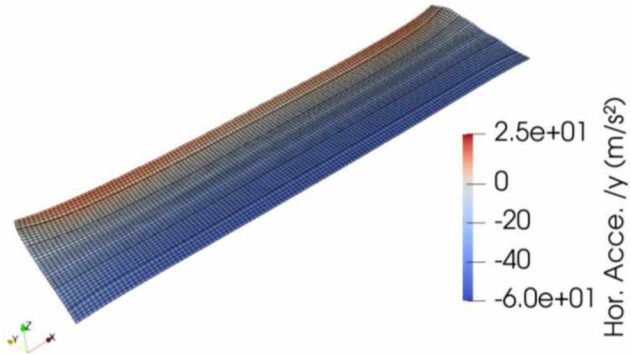

(b)

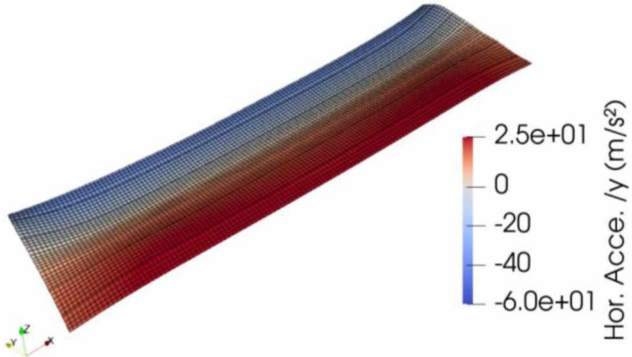

(c)

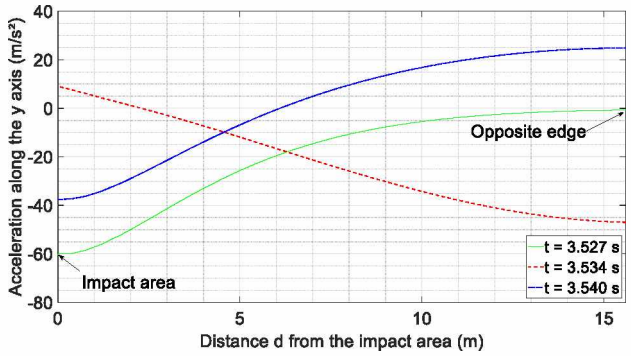

(d)

Figure 17 : Horizontal acceleration $\ddot{u}_y$ of nodes belonging to the 8th floor: t = 3.527 s (a), t = 3.534 s (b), t = 3.540 s (c), and evolution versus the distance d from the impact area (d).

The shock wave due to the force applied at time 3.527 s reaches the opposite edge of the building at time 3.534 s. At this point, the impact is still in progress. So, in addition to the instantaneous loading, there is a local stress concentration. The acceleration is thus greater at the opposite edge of the floor than close to the impact areas, despite the viscous damping reducing the acceleration in the high frequency range as the waves propagate. The same phenomenon appears at time 3.540 s, when the wave comes back, except that the stress due to the shock wave is opposed to the instantaneous loading, leading to a reverse of the sign of the acceleration close to the impact area.

Each reflection of a shock wave generates a local amplification of the stresses at the edge. To highlight this phenomenon, the evolution of the magnitude of the horizontal effort F_y is assessed on the entire 8th floor (*cf.* Figure 18).

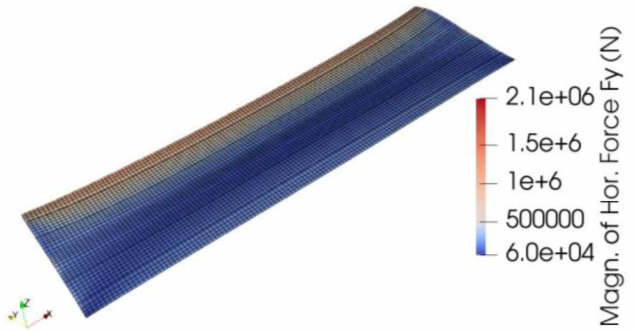

(a)

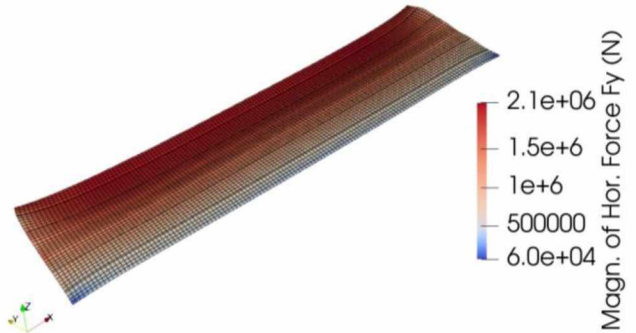

(b)

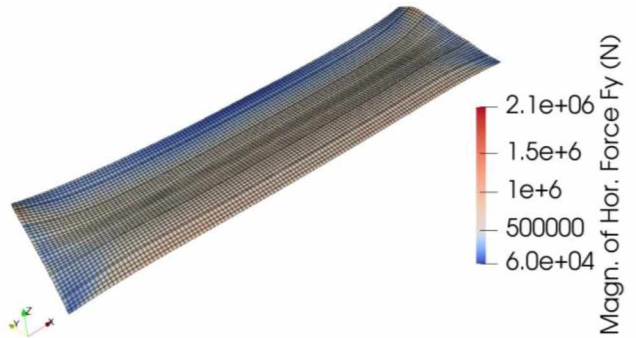

(c)

Figure 18 : Magnitude of the horizontal force F_y applied to the 8th floor: t = 3.527 s (a), t = 3,534 s (b) et t = 3,540 s (c).

Figure 18 (a) and Figure 18 (b) show that the main impact is still in progress at time 3.534 s, increasing the magnitude of the stresses applied to the 8th floor close to the impact area. But, at time 3.540 s, the impact is over, and a reflection happens (*cf.* Figure 18 (c)), increasing the magnitude of the stresses at the edges opposed to the impact area. As a result, the pseudo-acceleration spectra given by the SBMs are not conservative at floor level, the shock waves increasing considerably the response at the edges of the floor where reflections happen.

Note that contrary to the pseudo-acceleration FRS, the displacement FRS plotted in Figure 15 (a) do not vary significantly at the 8th floor level. This shows that the floors move as rigid bodies, which validates the rigid beam assumption used to model the floors in the SBMs (see Section 3.1).

4.3.2 Influence of floor height

The FRS assessed along the height of the building are detailed in Figure 19. The comparison is made by using the pseudo-acceleration at the impact areas, whereas FRS in Figure 10 and Figure 13 are computed at the centres of gravity of the floors (which explains the differences between the charts). The results show that the pseudo-acceleration computed at the impact area of the 7th floor increases abruptly above 33 Hz, to become the highest over the frequency interval [36 Hz, 152 Hz]. This phenomenon is due to the presence of an acceleration peak greater equal to 56 m/s² at the 7th floor (*cf.* Figure 20 (a)). This increases the content of the response in the high frequency range (*i.e.* when $f \geq 40$ Hz), as shown by the power spectral density (PSD) of the acceleration response (*cf.* Figure 20 (b)). In order to explain this amplification, a detailed study is performed in the following paragraphs.

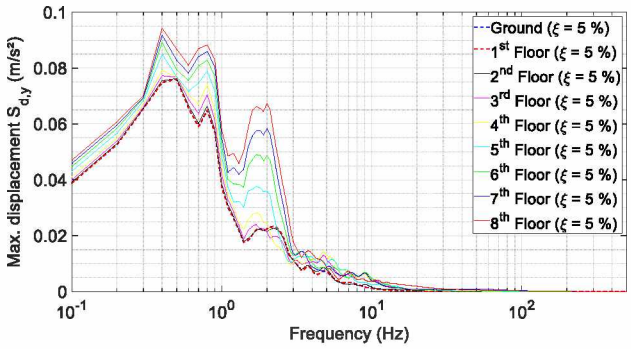

(a)

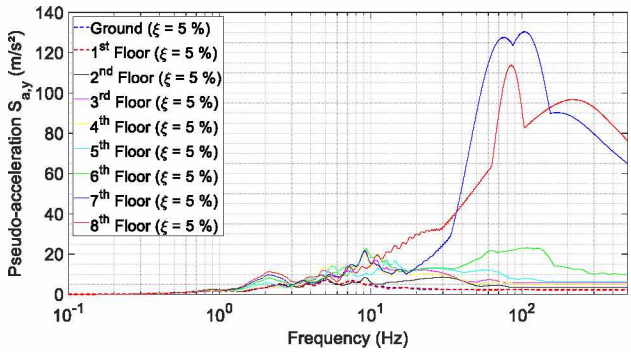

(b)

Figure 19 : FRS computed in the direction of $\boldsymbol{e}_y$ at impact areas (influence of floor height): displacement (a) and pseudo-acceleration (b).

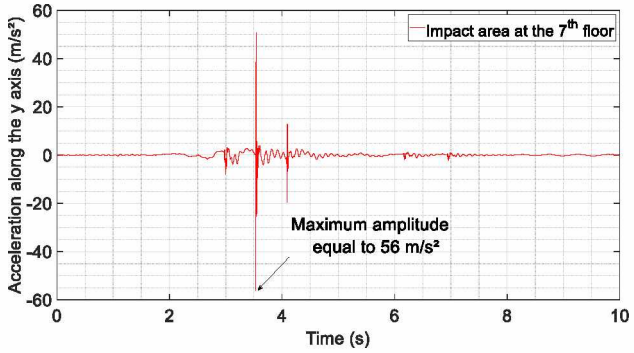

(a)

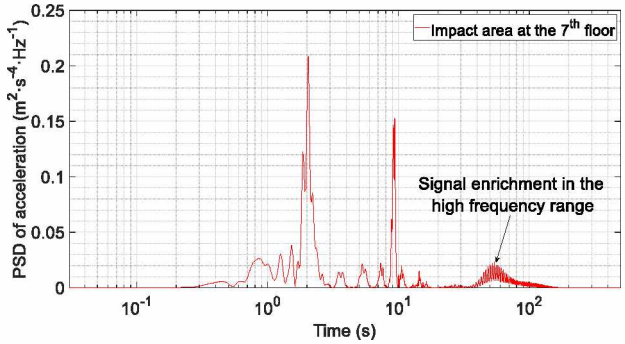

(b)

Figure 20: Acceleration in the direction of $\boldsymbol{e}_y$ at the impact area of the 7th floor versus time (impact area – a) and power spectral density of the acceleration response versus frequency (b).

Figure 21 shows that the PSD of the main impact force applied to the 8th floor is about 100 times higher than the PSD of the main impact force applied to the 7th floor. This difference is due to a higher number of impacts at the top of the buildings (each impact bringing a considerable amount of energy), even if the frequency contents of both loadings are mainly distributed over a frequency range worth between 0 and 100 Hz.

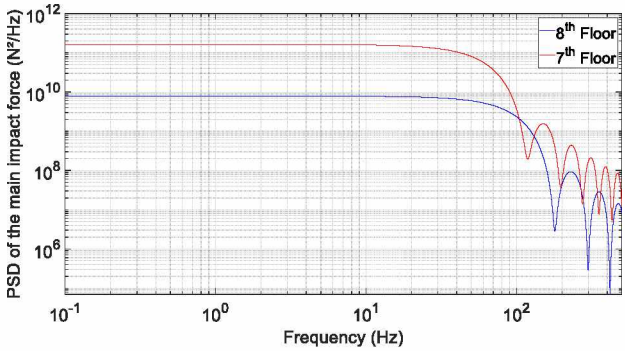

Figure 21 : PSDs of the main impacts applied to floors 7 and 8 versus frequency (logarithmic scale).

To understand how the impact forces are transmitted to the upper floors, the transfer functions linking the FFT (fast Fourier transform) of the acceleration response and the FFT of the impact forces are assessed in the frequency domain at the impact areas of the 6th, 7th and 8th floors (*cf.* Figure 22 (a) & (b)), but also at the top floor level (depending on the distance to the impact area – *cf.* Figure 22 (c)). Each one of them acts as a filter that modify the frequency range depending on the mechanical and geometrical properties of the structure.

The transfer functions are defined by three acceleration peaks related to the first bending modes about the $\boldsymbol{e}_x$ axis (*cf.* Figure 22 (b)). The high frequency behaviour shows that shock waves are not transmitted from floor to floor in case of multi-storey buildings, floors being stiffer than walls and columns in the presented case study. So, the amplification of the floor response in the high frequency range is mainly due to the loading directly applied to the floor. The blue curve in Figure 22 (a) shows that the acceleration response at the impact area of the 7th floor is very sensitive to loadings having a strong frequency content over the interval [50 Hz, 400 Hz]. This is the case of the impact force applied to the 7th floor, whose main frequency range is worth between 0 Hz and 100 Hz (*cf.* Figure 21). As a result, the frequency content of the acceleration response computed at the impact area of the 7th floor is high between 50 Hz and 100 Hz, explaining why a signal enrichment appears in Figure 20 (b).

Note that this is not the case of the impact area of the 8th floor, where the acceleration response is more sensitive between 85 Hz and 400 Hz (see red curve in Figure 22 (b)): the impact forces are thus transmitted to the floors via a shorter frequency interval (worth between 85 Hz and 100 Hz). In addition, the maximum value of the transfer function is equal to 1.5×10^{-6} kg^{-1} at the 8th floor, while the value 2.5×10^{-6} kg^{-1} is reached at the 7th floor. Knowing that the 8th floor is two times heavier that the 7th floor (*cf.* Appendix A), this could explain why it is less sensitive to impact forces. As a result, the pseudo-acceleration is the highest at the level of the impact area of the 7th floor between 36 Hz and 152 Hz (*cf.* Figure 19 (b)), although this floor undergoes weaker impacts.

Figure 22 (c) shows that the high frequency content is damped as the horizontal distance from the impact areas increases. This phenomenon is due to the Rayleigh damping, whose amplitude increases with respect to the frequency. As a result, the points located far away from the impact areas exhibit lower a pseudo-acceleration in the high frequency range, whereas their pseudo-acceleration is the highest beyond 75 Hz. However, note that considering that the three main bending eigenfrequencies (carrying 81 % of the mass above ground level - *cf.* Table 2) are worth between 1 Hz and 10 Hz and that the PSD of impact loading starts to decrease from 100 Hz (*cf.* Figure 21), the damping has little influence on the full response, explaining why the horizontal acceleration response in Figure 16 is anyway higher far from the impact area.

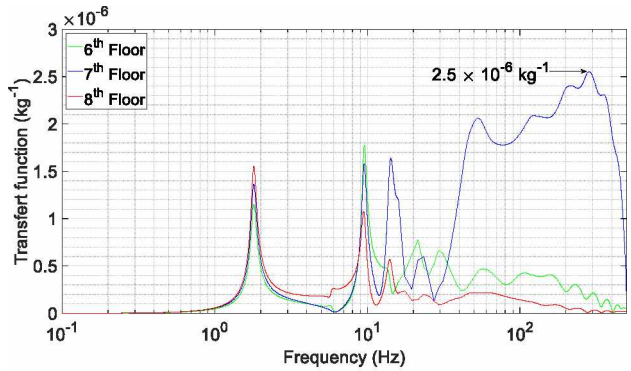

(a)

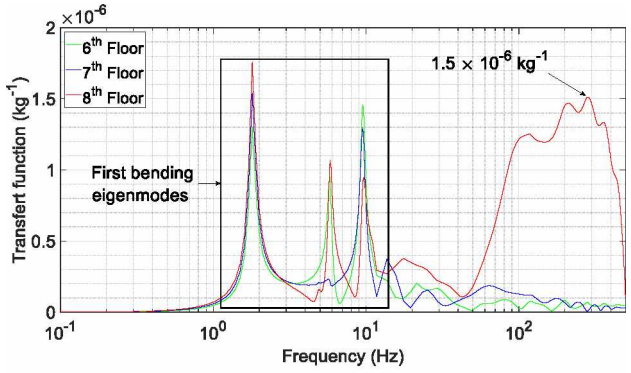

(b)

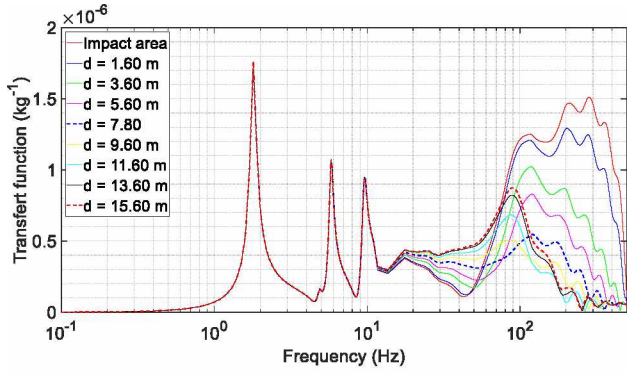

(c)

Figure 22 : Transfer functions computed at the impact areas of the 6th, 7th and 8th floors: loadings applied to the 7th floor (a) and 8th floor (b), and transfer functions computed at the top floor level (loading applied to the 8th floor- c).

5. Loading demand at the bottom of a device

5.1 Characteristics and location of the device

The "transferred spectra" are used in order to assess the response of the devices that can be modelled by SDOF oscillators. However, when these devices (pumps, chimneys, electrical cabinets, etc.) have several eigenmodes, other approaches must be used. Among them, implementing the devices on a 3D mesh of the building and carrying a detailed finite element analysis allows to

assess (at each time step) the forces applied to the device without cutting the high frequency content lower than half of the sampling frequency. This method is accurate but computationally demanding, and is generally used for verification purposes only. Being less consuming in CPU time, the response spectra analysis (RSA) allows to quickly assess the loading demands (*i.e.* the maximum external loads encountered by the devices) in order to adjust the properties of the devices and their anchors: this method is thus more suited for design purposes. In this case, the acceleration transmitted to the device is firstly post-processed from the results of a detailed finite element analysis performed on the 3D mesh of the building. Secondly, the eigenfrequencies and the eigenmodes of the device are computed. Thirdly, the FRS are built according to the modal damping applied to each eigenfrequency, and the influence of each eigenmode is assessed according to its effective modal mass. At last, the response is computed by applying SRSS (Square Root of the Sum of the Square) or CQC (Complete Quadratic Combination) methods.

The aim of this study is to assess the accuracy of the RSA method in case of earthquake induced pounding. For this purpose, a comparison with the results of detailed 3D finite element analyses is carried out on a device, and a sensitivity analysis depending on the high frequency damping ratio is proposed.

Note that the choice is made in this work to consider a fictious and generic device: its model has been set to be as general as possible, the study being focused here on the reliability of the RSA method. More accurate models should be used to design actual industrial devices (which is not the case in this study).

The device is located on the 8th floor of the first building, at the point of coordinates (23.1 m, 12.0 m, 30.3 m) (*cf.* Figure 23). The stiffness of the device is set in order to guarantee that the two first eigenmodes appear around 30 Hz and 80 Hz (typically representative of the modal characteristics of a pump). It is cylindrical in shape, 1 m high with a 50 cm radius, its mass centre is located at a height of 46 cm from the floor and its total mass is 1,500 kg.

The device (in red in Figure 24) is modelled by a beam element linked to its mass. The anchors (in green) are modelled by infinitely rigid Euler-Bernoulli beam elements linking the base of the device to the floor (in deep blue). A stiffness matrix is added between the base and the anchors to define the modal properties of the device (see orange elements in Figure 24). Here, the device can rotate about the $\boldsymbol{e}_x$ axis and translate in the $\boldsymbol{e}_y$ direction according to stiffnesses $K_{rxx} = 3.0\times10^7$ N.m/rad and $K_{yy} = 1.4\times10^8$ N/m. A kinematic relationship allows to extract the stresses at the base of the device as support reactions (see light blue elements in Figure 24). The modal characteristics of the device are detailed in Table 6, while the two first eigenmodes are computed in the $\boldsymbol{e}_y$ direction in Figure 25.

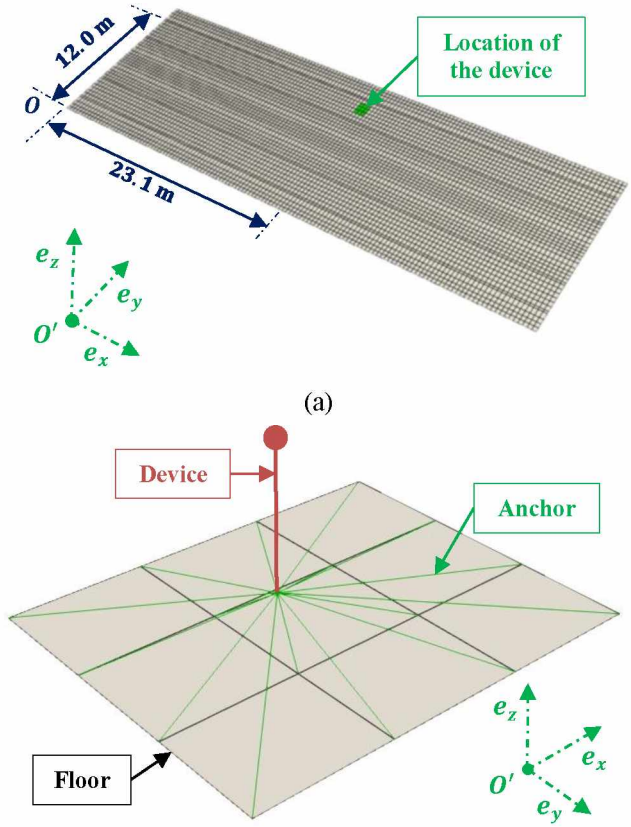

Figure 23 : Position of the device on the 8th floor (a) and connections to the floor (b).

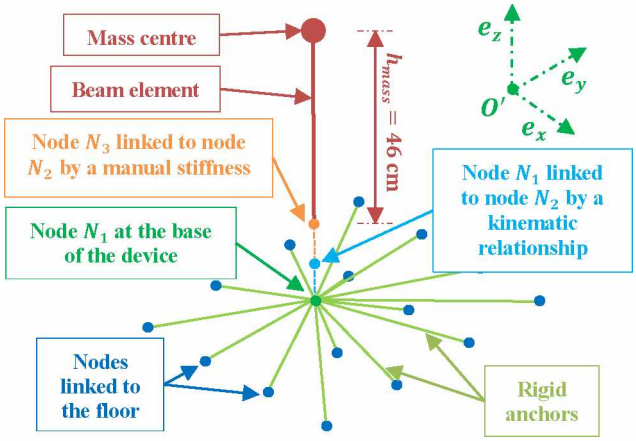

Figure 24 : Modelling of the device in Cast3M® finite element software.

Table 6 : Frequency and nature of the eigenmodes of the device.

Eigen mode	f (Hz)	Type/Direction	Modal effective mass (kg)
1	30.51	Bending about the $\boldsymbol{e}_x$ axis and translation in the $\boldsymbol{e}_y$ direction	1218.9
2	30.51	Bending about the $\boldsymbol{e}_y$ axis and translation in the $\boldsymbol{e}_x$ direction	1218.9
3	82.90	Bending about the $\boldsymbol{e}_x$ axis and translation in the $\boldsymbol{e}_y$ direction	327.0
4	82.90	Bending about the $\boldsymbol{e}_y$ axis and translation in the $\boldsymbol{e}_x$ direction	327.0

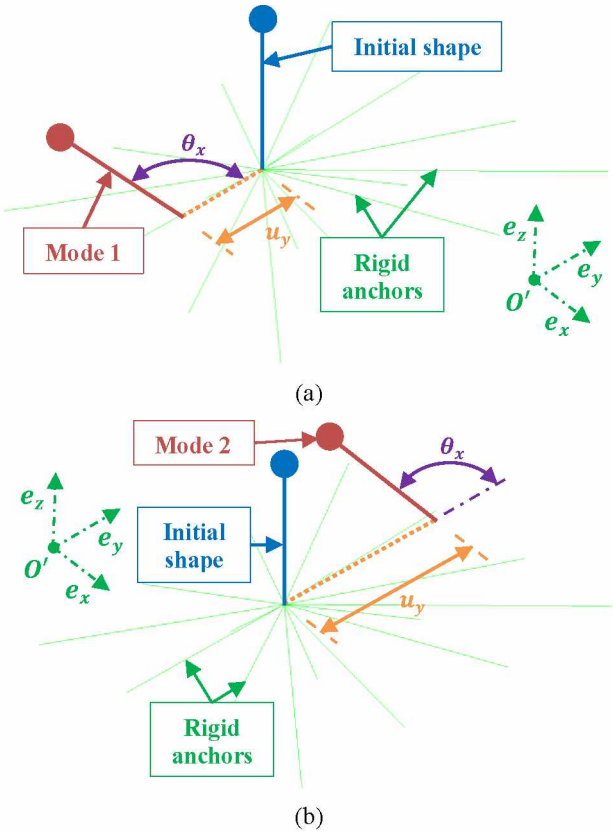

(a)

(b)

Figure 25 : First eigenmode - f_1 = 30.51 Hz (a) and second eigenmode – f_2 = 82.90 Hz (b).

The Figure 25 shows that the two first eigenmodes are defined by a rotation about the $\underline{\boldsymbol{e}}_x$ axis and a translation in the $\underline{\boldsymbol{e}}_y$ direction. These movements depend on the stiffnesses K_{rxx} and K_{yy} (*cf.* Figure 26). Note that the displacements related to bending are here negligible compared to the ones related to the rotation at the base of the device. According to the first eigenmode, translation and bending are oriented in the same direction (*cf.* Figure 25 (a)), whereas they are opposed with the next one (*cf.* Figure 25 (b)). The effective modal mass reaches 78.8 % of the total modal mass (*i.e.* 1545.9 kg) with the first eigenmode and 21.2 % with the second one (*cf.* Table 6).

The viscous damping of the device is modelled by a Rayleigh damping ratio set at 2 % at 30 Hz and 80 Hz (*i.e.* around the two first eigenmodes in the $\boldsymbol{e}_y$ direction).

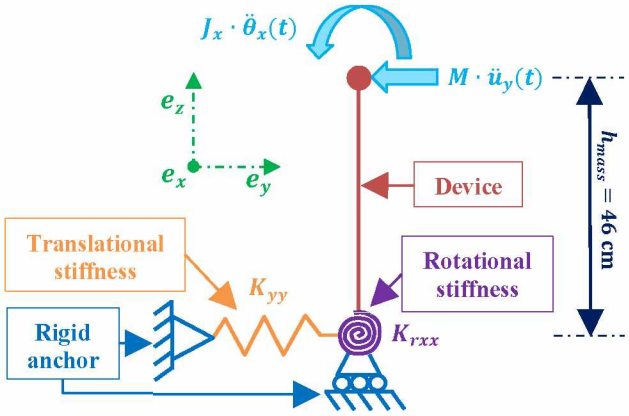

Figure 26 : Mechanical model of the device – elevation in the $(\boldsymbol{O}, \boldsymbol{e}_y, \boldsymbol{e}_z)$ plane.

5.2 *Calculation of the loading demand at the bottom of the device*

The forces and moments applied at the base of the device (N_x, F_y, F_z, M_x, M_y, M_z) are firstly computed from the results of a detailed finite element analysis, with and without impacts. In the framework of this study, only the shear force in the direction of $\boldsymbol{e}_y$ (called F_y) is assessed. Secondly, the maximum value of F_y (*i.e.* the loading demand) is compared with the result of a RSA. The shear force F_y is plotted in Figure 27 as a function of time (extracted from the results of a detailed finite element analysis). The loading demand and the pseudo-acceleration given by both methods are summarized in Table 7.

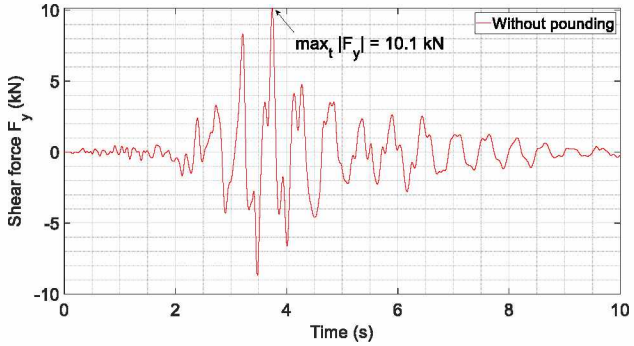

(a)

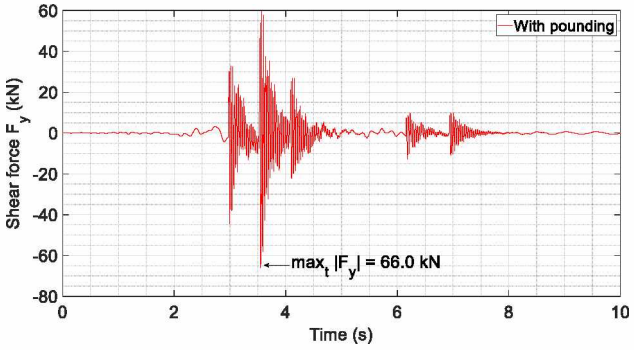

(b)

Figure 27 : Shear force in the $\boldsymbol{e}_y$ direction versus time: without impact (a) and with impacts (b).

Figure 27 (b) highlights that the loading due to the impacts being rich in the high frequency range, it stresses more the rigid device than the seismic loading (*cf.* Figure 27 (a)). As a result, high-frequency oscillations appear on the floor response, as shown by the "noisy" evolution of the shear force F_y.

Moreover, Table 7 show that the RSA underestimates the magnitude of the loading applied to the anchors. Indeed, the analysis is performed by using only two bending/shearing modes, whereas detailed finite element analysis allows to take into account of the entire frequency content up to half of the sampling frequency, in accordance with the Shannon's theorem. Results also highlight that the relative error between both methods is more important when the impact forces are not applied (reaching 34.6 % without impact against 2.7 % with impacts). This difference is mainly due to the nature of the FRS used to assess the loading applied to the device. Indeed, the FRS are defined according to the response in the $\boldsymbol{e}_y$ direction. However, the loads applied to the building also generate bending and torsion rotations at floor level. These movements are not taken into account in the RSA method, whereas they have a non-negligible influence when the building is only subjected to a seismic loading. To the contrary, the impact forces impose a horizontal movement to the upper floors, decreasing the influence of the rotations on the floor response: this explains why the results of the RSA method are closer to those given by the detailed finite element analysis when pounding is taken into account.

Table 7 : Results given by detailed finite element analysis and RSA.

	Without impact		With impacts	
	Detailed finite element analysis	RSA	Detailed finite element analysis	RSA
Loading demand $\max_t \lvert F_y \rvert$ (N)	10,143	6,633	66,028	64,272
Pseudo-acceleration $S_{a,y}$ (m/s²)	6.56	4.32	42.7	41.6

With a relative error less than 10 %, the results given by RSA are more accurate in case of pounding between adjacent structures. But it should be noted that envelope FRS needs to be used with RSA in order to not undersize the device under study. As carrying out a detailed finite element analysis on a 3D mesh is costly in computation time, this approach should only be used to validate the final design or peculiar points only.

Note that the Rayleigh viscous damping ratio applied to the structure has also a large influence on the response of the device in the high frequency range. This can increase the error between the results given by the RSA method and the detailed finite element analysis. To check this point, a sensitivity analysis needs to be carried out.

5.3 Influence of the damping ratio applied to the structure on the response of the device

The following study is led in order to assess the influence of the viscous damping ratio applied to the buildings. This includes the SBMs and the 3D mesh of the first building, so the restitution ratio and the impact forces are reassessed in each case (but note that the penalty stiffness is still equal to 10^{11} N/m). Three damping levels (under-damped, damped, and over-damped in the high frequency range) are compared (*cf.* Figure 28). The Rayleigh damping parameters and the restitution ratio are summarized in Table 8 for all three case studies. Note that the value of ε (reassessed as described in Section 3.2.2) increases as the value of the Rayleigh damping ratio decreases in the high frequency range. A sensitivity analysis could thus be carried out into a further study to assess the dependency of the restitution ratio ε on the damping parameters, the geometry, and the mechanical properties of a rectangular in shape floor.

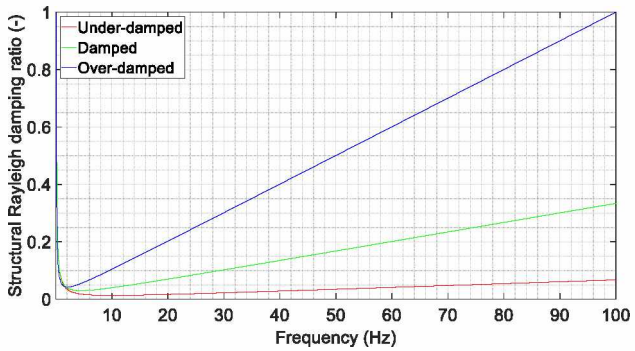

Figure 28 : Rayleigh damping ratios used in the sensitivity analysis.

Table 8 : Parameters defining the Rayleigh damping ratio applied to the structure and restitution ratio used to model the impacts between the SBMs.

	Under-damped	Damped	Over-damped
α_R (s^{-1})	0.838	0.838	0.559
β_R (s)	2.12×10^{-4}	1.06×10^{-3}	3.18×10^{-3}
ε (-)	0.414	0.687	0.891

The aim of this sensitivity analysis is to find whether decreasing the value of the damping ratio of the structure increases or decreases the error between the results given by the RSA and the detailed finite element analysis. To do so, the FRS in pseudo-acceleration are first computed at the base of the device with and without pounding, with a damping ratio set at 2 % (*cf.* Figure 29).

Figure 29 (a) shows that when no impact occurs, the PFA at the 8th floor increases as the damping ratio of the structure decreases (rising the value of the pseudo-acceleration). Figure 29 (b) also highlights that a low damping ratio in the high frequency range leads to an amplification of the floor response from 70 Hz onwards when impact occurs. Otherwise, when the structure is over-damped, the maximum pseudo-acceleration decreases (reaching 67.6 m/s² at 178 Hz, see blue curve in Figure 29 (b)). This shows that a low structural damping ratio leads to an amplification of the response of the device in the high frequency range around the second eigenmode (whose eigenfrequency is equal to 82.9 Hz).

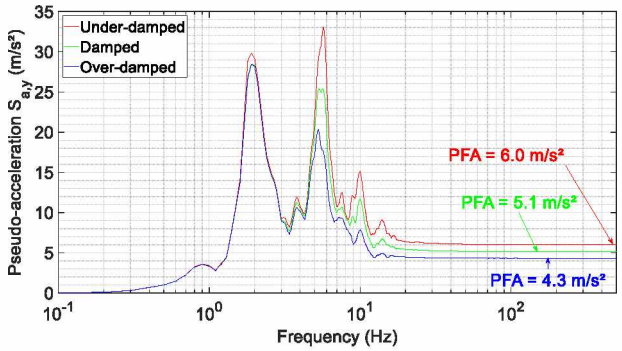

(a)

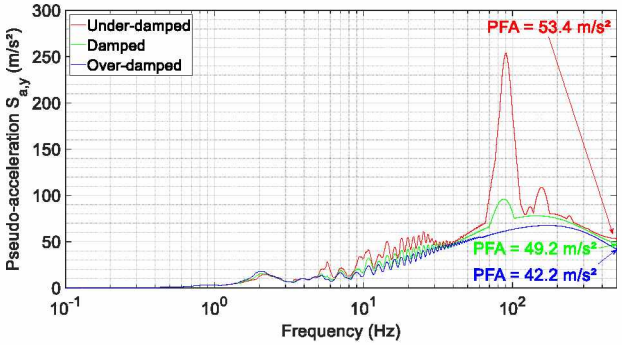

(b)

Figure 29 : FRS at the base of the device computed in the $\boldsymbol{e}_y$ direction: without pounding (a) and with pounding (b).

The loading demands given in the $\boldsymbol{e}_y$ direction according to the RSA and the 3D finite element analyses are detailed in Figure 30 and Table 9.

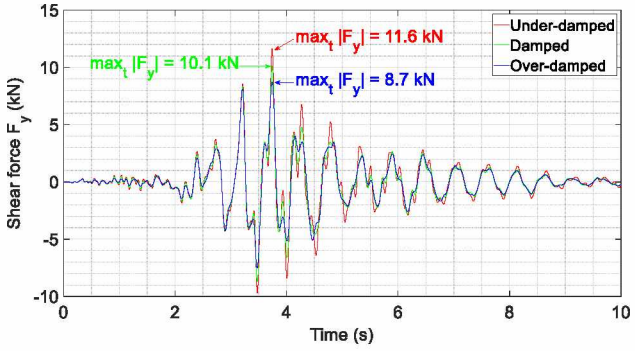

(a)

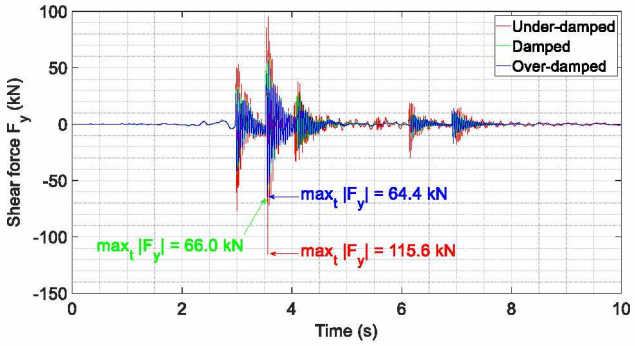

(b)

Figure 30 : Design loading in the $\boldsymbol{e}_y$ direction versus time: without impact (a) and with impact (b).

Figure 30 highlights that the shear force in the direction of $\boldsymbol{e}_y$ varies more when pounding is taken into account. Indeed, contrary to the seismic loading, impact forces enrich the high frequency content of the response, *i.e.* where the differences of damping are the highest.

Table 9 : Loading demands *given by RSA and detailed 3D finite element analyses.*

	Without impact			With impacts		
	Detailed finite element analysis (N)	RSA (N)	Relative difference (%)	Detailed finite element analysis (N)	RSA (N)	Relative difference (%)
Under-damped	11,614	7,795	32.9	115,580	90,060	21.6
Damped	10,143	6,633	34.6	66,028	64,272	2.7
Over-damped	8,725	5,512	36.8	64,432	57,157	11.3

Table 9 compares the results given by detailed 3D finite element analyses and RSA. As previously shown, the error between both methods is higher when pounding is not taken into account, the movements of the floors being as much caused by rotations as by translations. The relative error is also much more sensitive to the damping when impact forces are applied to the building (its value being worth between 2 % and 22 %). Note that the relative error seems to strongly increase when the structure is under-

damped (even if a rise can also be observed when the structure is over-damped). This shows that the accuracy of the results given by the RSA method may vary according to the damping applied to the structure in case pounding is taken into account. So, the choice of the Rayleigh damping ratio is important, its value having a great influence on the response of the devices. It is common to use a Rayleigh damping ratio less than or equal to 7 % around the main eigenmodes in order to perform linear finite element analyses on reinforced concrete structures [26]. Here, this choice leads to a restitution ratio worth between 0.6 and 0.7. Despite these errors, the same order of magnitude is achieved whatever the method used, showing that the RSA can be used to design the devices and their anchors if envelope FRS are used (in order to avoid under-sizing).

6. Conclusions

In this paper, the influence of earthquake induced pounding on FRS in case pounding occurs between two adjacent multi-storey buildings is discussed. To do so, the impacts are modelled by using a penalty method on SBMs having the same modal characteristics as the ones of the buildings. The impact forces are then applied on a 3D mesh of the first structure made from shell and beam elements. Local FRS are computed along the height of the building and at the top floor level, and the reliability of the RSA method (allowing for the calculation of the loading demand of the bottom of the devices) is assessed.

Firstly, the results showed that local amplifications of the FRS appear at the edges of the floors due to the propagation and reflections of shock waves. An analysis based on transfer functions highlighted that the response of the floors depends on the frequency content of the impact forces as well as the mechanical properties of the buildings (masses, stiffnesses, geometry, etc.). The damping of the shock waves in the high frequency range (due to the Rayleigh damping) was also noticed.

Secondly, a comparison between detailed 3D finite element analyses and RSA was carried out by adding a device on the last floor. Results proved that when pounding is taken into account, the relative error between both methods decreases due to the horizontal movement imposed by the impacts, even if the RSA method underestimates the loading demand. So, the use of the RSA method to design devices is viable as far as pounding envelope FRS are used. In addition, a sensitivity analysis showed that the response of the devices depends strongly on the value of the Rayleigh damping ratio applied to the structure in the high frequency range, highlighting that its choice increases uncertainties. The reassessment of the restitution ratio finally proved that its value is strongly dependent of the damping applied to the floors of the 3D mesh: to correctly compute the impact forces with the SBMs, it is thus necessary to find beforehand the best value of ε by modelling one (or several) impacts on the 3D mesh by using the LCP method. To do so, a method based on a pre-computation on the 3D mesh was proposed.

In this paper, the method used to model pounding can only be applied to simple case studies, *i.e.* parallel multi-storey buildings with adjacent floors. In order to model geometrical defects (such as parallelism) or non-planar impact areas (*e.g.* circular in shape), an improvement of the SBM consisting in modelling the geometry of the floors with horizontal rigid bars is under study. A sensitivity analysis based on the Rayleigh damping parameters, geometry, and mechanical properties of the materials will also be

carried out on several floors in order to create a tool allowing for an easier assessment of the penalty parameters used to model the impacts on the SBMs.

Acknowledgements

The authors wish to express their most grateful thanks to IRSN for its financial and technical support and to the members of the civil engineering expertise office.

References

[1] NF-EN-1998. Conception et dimensionnement des structures pour leur résistance au séisme; 2004. (In French).

[2] O'Hara G. Impedance and shock spectra. The Journal of the Acoustical Society of America 1959;10(31):1300-1303.

[3] O'Hara G. Shock spectra and design shock spectra. Naval Research Laboratory Technical Library; 1959.

[4] Kelly J M, Sackman JL. Shock spectra design methods for equipment in impulsively loaded structures. Defense Nuclear Agency; 1979.

[5] Anagnostopoulos S. Pounding of buildings in series during earthquake. Earthquake Engineering and Structural Dynamics 1988;16:443-445.

[6] Anagnostopoulos S. Equivalent viscous damping for modeling inelastic impacts in earthquake pounding problems. Earthquake Engineering and Structural Dynamics 1992;33:897-902.

[7] Papradrakakis M, Mouzakis H, Plevris N, Bitzarakis S. A Lagrange multiplier solution method for pounding of buildings during earthquakes. Earthquake Engineering and Structural Dynamics 1991;20:981-998.

[8] Muthukumar S, Desroches R. A Hertz contact model with non-linear damping for pounding simulation. Earthquake Engineering and Structural Dynamics 2006;35:811-828.

[9] Acary V, Brogliato B. Numerical methods for Nonsmooth Dynamical System. Montbonnot: Springer; 2008.

[10] Acary V. Energy conservation and dissipation properties of time integration methods for nonsmooth elastodynamics with contacts. Journal of Applied Mathematics and Mechanics 2016;96(5):585-603.

[11] Crozet V, Politopoulos I, Chaudat T. Shake table tests of structures subject to pounding. Earthquake Engineering and Structural Dynamics 2019;47:219-235.

[12] Crozet V, Politopoulos I, Yang M, Martinez J-M, Erlicher S. Sensitivity analysis of pounding between adjacent structures. Earthquake Engineering and Structural Dynamics 2018;47:219-235.

[13] Langlade T, Bertrand D, Grange S, Candia G. Modélisation 2D d'entrechoquement de structures par une méthode de complémentarité. 10ème Colloque National AFPS; 2019. Strasbourg, France. (In French).

[14] Jameel M, Saiful Islam A, Rizwan Hussain R, Danish Hasan S, Khaleel M. Non-linear FEM analysis of seismic induced pounding between neighbouring multi-story structures. Latin American Journal of Solids and Structures 2012;10:921-939.

[15] Mahmoud S, Abd-Elhamed A, Jankowski R. Earthquake-induced pounding between equal heights multi-story buildings considering soil-structure interaction. Bulletin of Earthquake Engineering 2013;11:1021-1048.

[16] Yang Y, Li S. Development of a refined analysis method for earthquake-induced pounding between adjacent RC frame structures. Sustainability 2019;11(18):4928.

[17] Zhang Y, Ding J, Zhuang H, Chang Y, Chen P, Zhang X, Fan J. Pounding between adjacent frame structures under earthquake excitation based on transfer matrix method of multibody systems. Advances in Civil Engineering 2019;2019:1-31, Article ID 5706015.

[18] Mazza F, Labernada R. Magnetic damped links to reduce internal seismic pounding in base-isolated buildings. Bulletin of Earthquake Engineering 2020;18:6795-6824.

[19] Mazza F, Labernada R. Internal pounding between structural parts of seismically isolated buildings. Journal of Earthquake Engineering 2021.

[20] Ministère du développement durable, BRGM. Plan séisme 2018. < http://www.planseisme.fr/Zonage-sismique-de-la-France.html >. (In French).

[21] Crozet V. Étude de l'entrechoquement entre bâtiments au cours d'un séisme. PhD thesis. ENS Cachan; 2019. (In French).

[22] Do TN, Filippou FC. A damage model for structures with degrading response. Earthquake Engineering and Structural Dynamics 2019;47(2):311-332.

[23] Mazza F. A plastic-damage hysteretic model to reproduce strength stiffness degradation. Bulletin of Earthquake Engineering 2019;17:3517-3544.

[24] Kotronis P, Grange S. Simplified modelling strategies for reinforced concrete structures. European Journal of Environmental and Civil Engineering, Taylor & Francis, 2011, 14 (6-7).

[25] Langlade T. Vulnerability and risk of structures subjected to earthquake induced pounding with a non-smooth contact dynamic method. PhD thesis. INSA Lyon; 2021. (In French).

[26] ASN/GUIDE/2/01. Prise en compte du risque sismique à la conception des ouvrages de génie civil d'installations nucléaires de base à l'exception des stockages à long terme des déchets radioactifs. Autorité de sûreté nucléaire 2006. (In French)

[27] Rayleigh BJWS. The theory of sound, Volume 2. London: Macmillan; 1896.

[28] Richard B, Martinelli P, Voldoire F, Chaudat T, Abouri S, Bonfils N. SMART 2008: Overview, synthesis and lessons learned from the international Benchmark. Engineering Structures 2016;106:166-178.

[29] Caughey TK, O' Kelly MEG. Classical normal modes in damped linear dynamic systems. Journal of Applied Mechanics (ASME) 1960;32:583-8.

[30] Nigam N, Jennings P. Digital calculation of response spectra from strong-motion earthquake records. Pasadena, California: California Institute of Technology; 1968.

Appendix A: Properties of the SBM of the first building

Floor	M (t)	J_x (kg·m²)	J_y (kg·m²)	J_z (kg·m²)	I_x (m^4)	I_y (m^4)	I_z (m^4)	A (m^2)	A_{vy} (m^2)	A_{vz} (m^2)
1	2502	6.3×10^7	5.1×10^8	5.7×10^8	6.4×10^3	4.2×10^4	4.8×10^4	234	169	214
2	1787	4.1×10^7	3.3×10^8	3.7×10^8	3.1×10^3	1.3×10^4	1.8×10^4	67	11	62
3	1682	4.1×10^7	3.3×10^8	3.7×10^8	3.1×10^3	1.4×10^4	1.7×10^4	69	11	62
4	1882	4.5×10^7	3.7×10^8	4.1×10^8	3.1×10^3	1.4×10^4	1.7×10^4	69	14	62
5	1680	4.4×10^7	3.3×10^8	3.8×10^8	3.3×10^3	1.6×10^4	1.9×10^4	73	17	62
6	1580	4.0×10^7	3.0×10^8	3.4×10^8	3.0×10^3	1.1×10^4	1.4×10^4	64	8	62
7	1574	4.0×10^7	3.2×10^8	3.6×10^8	3.0×10^3	1.1×10^4	1.4×10^4	64	8	62
8	3014	6.8×10^7	5.6×10^8	6.3×10^8	3.3×10^3	1.8×10^4	2.1×10^4	77	15	55